5G-OPERA Deliverable 5.3

Positioning

Document Properties	
Name of project	5G-OPERA
Document title:	Positioning
Client:	Ministère de l'économie, des finances, et de la relance, Bundesministerium für Wirtschaft und Energie
Official reference:	5G-OPERA D5.3
Reviewer:	WP5.3 team
Abstract:	On the RAN side, we implemented the signals, procedures and estimation algorithms to support 5G NR positioning. We make use of either UL or DL based positioning based on Time Difference of Arrival (TDoA) and we will implement the corresponding signals and procedures in OAI. In the DL, this can be achieved using the Downlink Positioning Reference Symbols (PRS) (Rel. 16) whereas in the UL this can be achieved using the UL Sounding Reference Symbols (SRS) as specified in Rel. 15 (Fraunhofer IIS, Eurecom & TU-D.). CEA-LETI addressed the issue of localisation in difficult environments and with narrowband signals (e.g., NB IoT). CEA use ML algorithms applied to a variety of received signal features (TDoA, fading) to extract relevant information w.r.t. location.
Date of publication:	20/12/2024
Version:	1.2
Access:	Internal
Keywords:	Open RAN, 5G Private Networks, Positioning

Table of Contents

1 Introduction

The **5G-OPERA** project aims to build a Franco-German ecosystem for private 5G networks under the joint leadership of TU Dresden and EURECOM (Sophia Antipolis). The focus of the project is the idea of open hardware and software with open interfaces in the area of mobile communication networks to allow multi-vendor options for technical equipment. The goal of the project is to ensure that the hardware and software of all project partners can work together. In addition to setting up reference test environments and demonstrators in Industry 4.0 environments, **5G-OPERA** is supporting the trials in the three demonstration projects and will advise all additional projects joining the program. For this report we focus on the improvements of positioning features during this project.

On the RAN side, we implemented the signals, procedures and estimation algorithms to support 5G NR positioning. We make use of either UL or DL based positioning based on Time Difference of Arrival (TDoA) and we will implement the corresponding signals and procedures in OAI. TDoA methods measure the time difference of the reference signals received by the UE in DL or at the base stations in UL and use their precise timing to estimate the location of the UE. In the DL, this can be achieved using the Downlink Positioning Reference Symbols (PRS) (Rel. 16) whereas in the UL this can be achieved using the UL Sounding Reference Symbols (SRS) as specified in Rel. 15 (Fraunhofer IIS, Eurecom & TU-D.). Eurecom developed techniques for handling multipath propagation, which complicates most positioning techniques; also, the precision of narrowband scenarios is improved by aggregating multiple carriers/bands. Finally, the exploitation of multiple antennas will be pursued to improve positioning precision, possibly by working in beam space.

CEA-LETI addressed the issue of localisation in difficult environments and with narrowband signals (e.g., NB IoT). CEA use ML algorithms applied to a variety of received signal features (TDoA, fading) to extract relevant information w.r.t. location. These algorithms learn to recognize situations such as obstructions, and to find the adequate correction to the estimated position.

2 Positioning in 5G NR and NB-IoT Overview

2.1 Concept phase

CEA-Leti addresses the challenge of positioning within Narrowband Internet of Things (NB-IoT) 5G networks, a technology used to deploy Low Power Wide Area Networks (LPWAN). The developed algorithms, integrated into the LMF, are based on the uplink time difference of arrival (UL-TDOA) scheme, similar to those used by other partners. CEA-Leti specifically aims to improve positioning performance in the context of NLOS propagation, which is frequently encountered in urban or peri-urban scenarios.

UL-TDOA localization of a User Equipment (UE) requires multiple valid measurements with gNB (3 in 2D, 4 in 3D) to compute a position. However, in urban or peri-urban scenarios, buildings may obstruct direct transmissions between the UE and gNB, resulting in only reflected signals being received. This reflection causes a significant bias in the propagation time due to the extra distance traveled by the signal. For instance, as illustrated in Figure 3, the LOS propagation between the UE and gNB #3 is blocked by building B1, and only the reflected signal traveling distance d3B is received. Additionally, even when the direct path is received, it may be biased by reflected signals from various obstacles. This is shown in the transmission between the UE and gNB #2 in Figure 1, where the received signal is a mix of the a transmission travelling distance d_{2A} and d_{2B}.

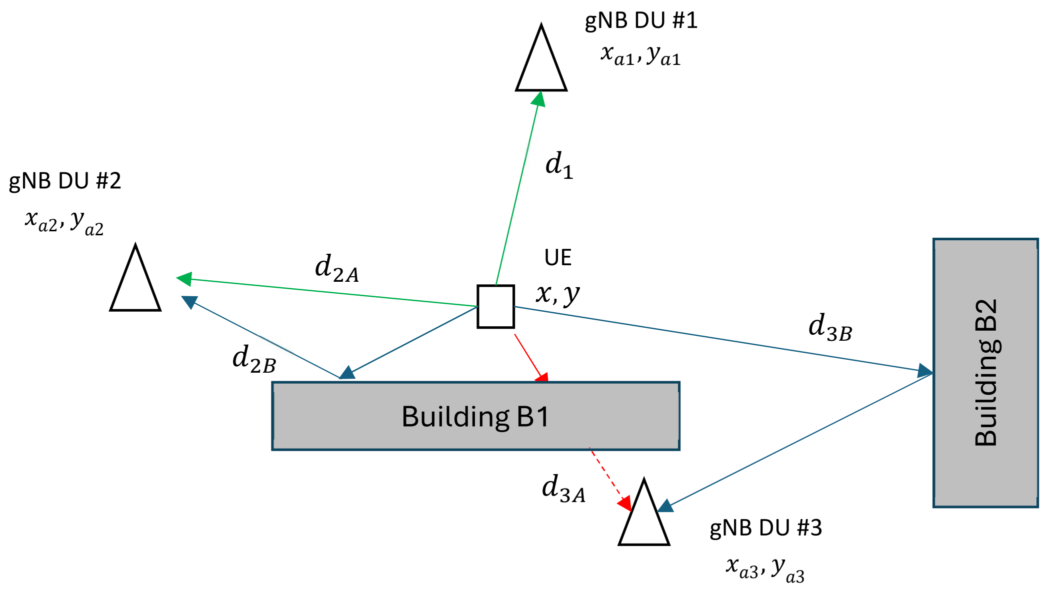

Figure 1 : illustration of urban scenario where buildings may block the direct propagation between UE and gNB.

Many of the State-of-the-art techniques used to overcome limitations in such environments relies on measurements redundancy, which permit to detect and discard or correct biased measurements. However, in the scope of 5G positioning, such approaches are not tractable

because it requires a network with high density of base stations, but this implies deployment cost that are significantly higher for limited benefits for the user.
Therefore, CEA-Leti proposes a new approach to improve accuracy and robustness for 5G positioning in challenging environments, while preserving the infrastructure complexity. This approach uses meta-information, such as 3D maps of buildings, to identify signals that may have been affected by complex propagation. Knowledge of the presence of obstacles on the path of a given transmission is used to weight the corresponding measurement as illustrated in Figure 2.

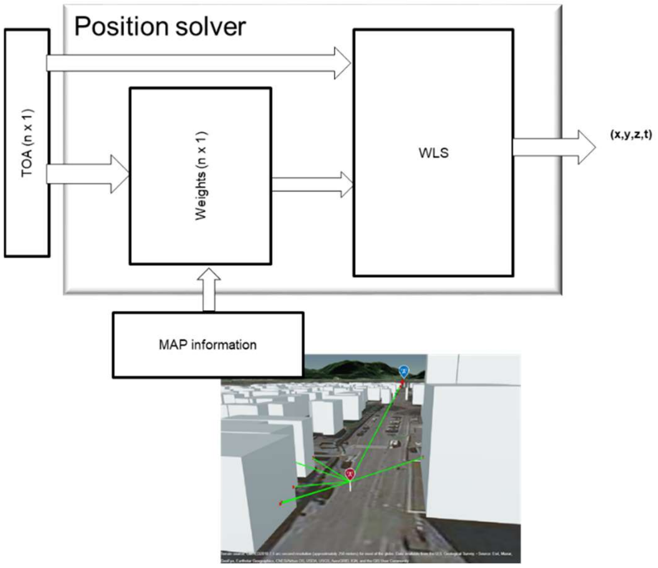

Figure 2 : Position solver architecture based on map information.

To analyze propagation using map information, like with ray tracing tools, it is necessary to know the positions of both the Base Station (gNB) and the User Equipment (UE). This creates a paradox: the UE's position is required to calculate its position.
To address this issue, we will test a set of predefined positions, selected on a grid. The algorithm will evaluate the likelihood of each predefined position based on the received measurements and map information, assigning a score to each. This approach allows the predefined positions to be used in processing the map data. Finally, an estimator will determine the final solution based on the scores of all tested positions. The architecture of the overall positioning algorithm is illustrated in the following diagram (Figure 3).

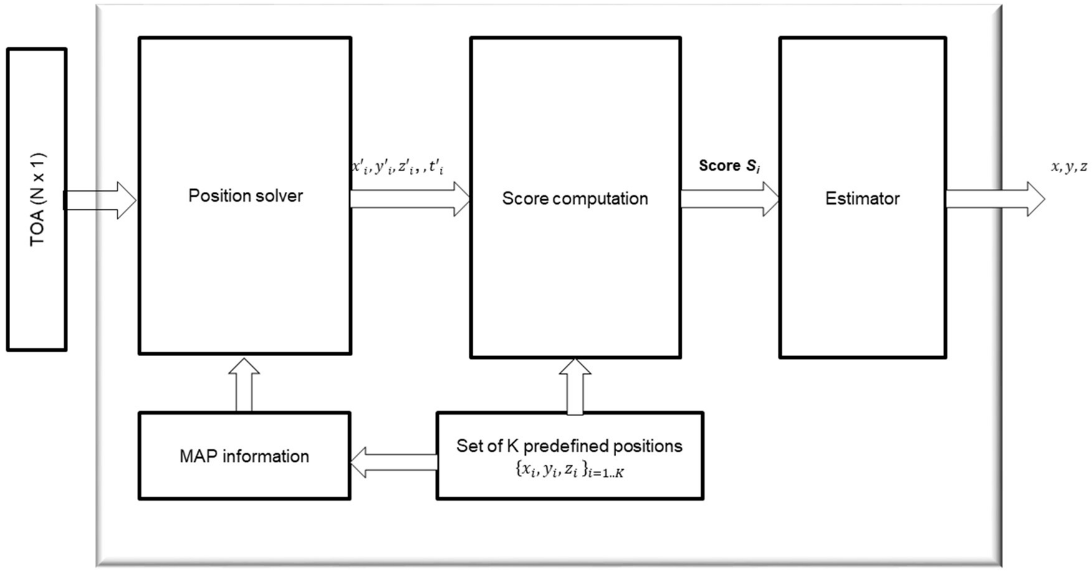

Figure 3 : Global architecture of the positioning algorithm.

Predicting signal propagation from 3D models is highly challenging. To tackle this, we tested two approaches : the "single ray" method and the "artificial intelligence" method.
The "single ray" method relies on LOS and NLOS information, utilizing a single-ray tracing technique and a maximum likelihood estimator (MLE). In contrast, the "artificial intelligence" method analyzes more complex features using advanced AI techniques.

2.1.1 Single-ray approach

This approach uses a simple propagation model based on a single ray between the gNB and the UE to determine if the propagation conditions are in LOS or NLOS, assuming that the former will have lower errors than the latter.

A. Measurement model

Localization based on TOA measurements requires that all receiving gNB are synchronized which is the case in 5G networks. However, such a synchronization cannot be assumed for UE whose departure time t_0 is unknown and must be estimated in addition to the position. Hence, we consider an UE at position $\mathbf{r} = [x \quad y \quad z]^T$ that performs some measurements with gNB at positions $\mathbf{r_b} = [x_b \quad y_b \quad z_b]^T$.
TOA measured with respect to a gNB can be modelled as

$$T_b = h(\mathbf{r}, t_0, \mathbf{r}_b) + \nu \qquad \text{Eq. 2.1}$$

with

$$h(\mathbf{r}, t_0, \mathbf{r}_b) = \frac{1}{c}\sqrt{(x - x_b)^2 + (y - y_b)^2 + (z - z_b)^2} + t_0 \qquad \text{Eq. 2.2}$$

where t_0 is the unknown departure time of the signal and ν a Gaussian distributed random variable that represents all the errors of the measurement process, including gNB related errors (e.g. synchronisation errors, time of arrival detection uncertainty) but also channel errors due to multipath and NLOS propagation. Although channel is essentially static and thus, channel errors are highly correlated over time (i.e. channel errors are biased), here we are considering their spatial distribution that we assume to be independent from one position to another (i.e. $\mathrm{E}\left(T_i, T_j\right) = 0$ for j ≠ j). In the general case, we shall assume that the error distribution is different for every considered position **r** because propagation conditions vary which makes the accuracy difficult to predict. We also assume that the TOA error distribution measured by a gNB when transmitter is located at position **r** depends only on the channel conditions between these two points:

$$\nu \sim \begin{cases} N(0, \sigma_{LOS}^2) & if \ = 1 \\ N(0, \sigma_{NLOS}^2) & if \ \delta_{LOS}(\boldsymbol{r}, \boldsymbol{r_b}) = 0 \end{cases} \qquad \text{Eq. 2.3}$$

with $\delta_{LOS}\left(\boldsymbol{r}, \boldsymbol{r_g}\right)$ a function that is equal to 1 if the positions $\boldsymbol{r}$ and $\boldsymbol{r_b}$ are in LOS, and 0 otherwise. Motivations for distinguishing between these two cases are that, in NLOS situations, the direct path of the radio wave can be blocked (e.g. by a building) and only reflected signals are received by the gateway. Because reflected signals travel longer distances than the direct path, the effective time-of-flight (TOF) experiences an excess delay resulting in a stronger TOA error than for direct propagation.
Therefore, positioning problem can be formulated as

$$\hat{\mathbf{r}}_{\boldsymbol{k}} = \arg\min p_{\bar{\mathbf{r}}_{\boldsymbol{k}}}(\mathbf{r}, T_1, \dots, T_N) \qquad \text{Eq. 2.4}$$

with

$$p_{\bar{\mathbf{r}}_{\boldsymbol{k}}}(\hat{\mathbf{r}}_{\boldsymbol{k}}, T_1, \dots, T_N) = \sum_{i=1}^{N} \left(\frac{T_b - h(\hat{\mathbf{r}}_{\boldsymbol{k}}, \hat{t}_{0,k}, \mathbf{r}_b)}{\sigma_{Los/NLOS}(\bar{\mathbf{r}}_{\boldsymbol{k}}, \mathbf{r}_b)} \right)^2 \qquad \text{Eq. 2.5}$$

B. Algorithm

As explained before, the main difficulty with the computation of the solution of Eq. 2.4, is that it depends on the true position to determine the value of $\sigma_{Los/NLOS}(\mathbf{r}, \mathbf{r}_b)$. Our approach consists in computing the maximum likelihood $p_{\bar{\mathbf{r}}_{\boldsymbol{k}}}(\hat{\mathbf{r}}_{\boldsymbol{k}}, T_1, \dots, T_N)$ assuming given positions from a set $\bar{\mathbf{r}}_{\boldsymbol{k}} \in \{\bar{\mathbf{r}}_{\boldsymbol{k}}\}_{\boldsymbol{k=1..K}}$. Typically, tested positions are chosen on a grid of possible UE positions, typically spanning a city with a step of e.g. 10m.
The score for each of the tested solution is computed using

$$S_k = p_{\bar{\mathbf{r}}_{\boldsymbol{k}}}\left(\hat{\mathbf{r}}_{\boldsymbol{k}}, \hat{t}_{0,k}, T_1, \dots, T_N\right) + \ (\hat{\mathbf{r}}_{\boldsymbol{k}} - \bar{\mathbf{r}}_{\boldsymbol{k}})^T P_0^{-1} (\hat{\mathbf{r}}_{\boldsymbol{k}} - \bar{\mathbf{r}}_{\boldsymbol{k}}) \qquad \text{Eq. 2.6}$$

with P_0 a 3x3 symmetric matrix that is used to weight the mismatch between the tested position $\bar{\mathbf{r}}_{\boldsymbol{k}}$ and the computed position $\hat{\mathbf{r}}_{\boldsymbol{k}}$**.**
For instance, P_0 could be a diagonal matrix such as

$$P_k = \begin{bmatrix} \sigma_x^2 & 0 & 0 \\ 0 & \sigma_y^2 & 0 \\ 0 & 0 & \sigma_z^2 \end{bmatrix} \qquad \text{Eq. 2.7}$$

In that case, diagonal coefficients σ_x^2, σ_y^2 and σ_z^2 are used to tune the mismatch tolerance for each of the coordinates. If they are set to $\sigma_x = 1$m, $\sigma_y = 2$m and $\sigma_z = 3$m, this would mean that a mismatch of the same or smaller magnitude than these values on each coordinate will result on a high score, but a larger mismatch will quickly drop it to a low value.
Also, to speed-up the algorithm, the visibility indicators $\delta_{LOS}(\boldsymbol{r_i}, \boldsymbol{r_b})$ are pre-computed for all positions from that grid, using single ray-tracing. Results of this precomputation is simply the so-called visibility map (see Figure 4), which indicates for each point from that grid the visibility value with respect to a given gNB.

Figure 4 : Example of visibility map for a base station (green indicates LOS propagation, red NLOS)

The algorithm computes the probability of each tested point to be the UE position by evaluating Eq. 2.5 given a set of TOA measurements. Figure 5 shows an example of probability map computed for the city of Grenoble, France, from 5 TOA measurements.

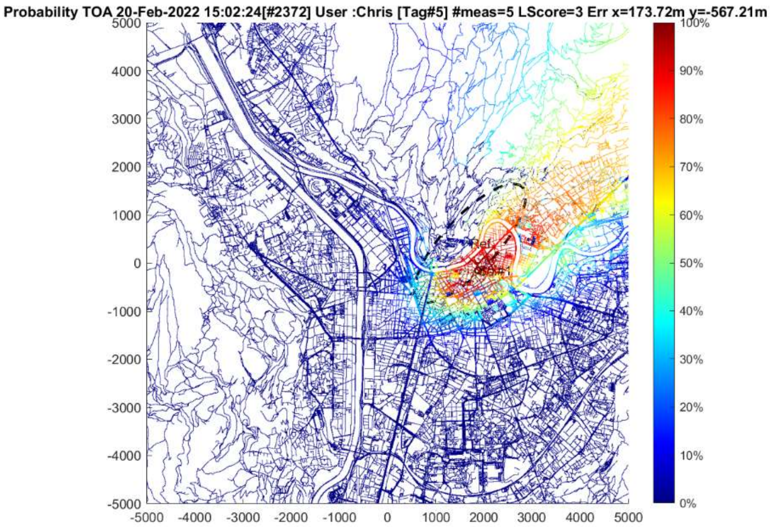

Figure 5 : Example of probability map computed for the city of Grenoble, France, from a set of 5 measurements.

It shows a region with high probability (in red) that includes the true position obtained from GNSS receiver.

Finally, the estimator block computes the final position which is output from the algorithm. It can simply output the position having the highest score, in that case it corresponds to a *Maximum a posteriori* (MAP) Estimator or it computes the mean value of all positions weighted by their scores

$$\hat{\mathbf{r}} = \frac{1}{\sum_{k=1}^{K} S_k} \sum_{k=1}^{K} \bar{\mathbf{r}}_{\boldsymbol{k}} \, S_k \qquad \textit{Eq. 2.8}$$

2.1.2 Artificial Intelligence based approach

The single-ray approach is limited to a simple model of the propagation conditions, where only the LOS / NLOS indicator is taken into account. However, real propagation may be much more complex, with e.g. only weak NLOS propagation that does not affect the direct path and does not result into a strong error, or, at the opposite, LOS situations that are mixed with reflected signals that cause poor measurements.

In this approach, we try to improve the prediction of the signal quality from a map using AI. Underlying idea is that, without simulating a complex propagation, an AI can infer this quality from the surrounding environment if it has learned it from similar configurations.

A. System architecture

The algorithm processes two types of information to predict weights ω_i associated to a TOA T_i . The first type of information comprises the per-link features, which are exclusively related to measurement T_i remain independent from other measurements. These features encompass map attributes describing the propagation of the corresponding link, as well as other metrics such as Received Signal Strength (RSS) and gNB height.

The second type of features consists of joint features that encapsulate relative information among all measurements, proving highly effective in identifying poor measurements. This concept resembles a consistency test of the solution, akin to conventional outlier detection techniques, but tailored to AI. While state-of-the-art approaches often overlook per-link features atop consistency tests, our proposed method amalgamates all available information through AI.

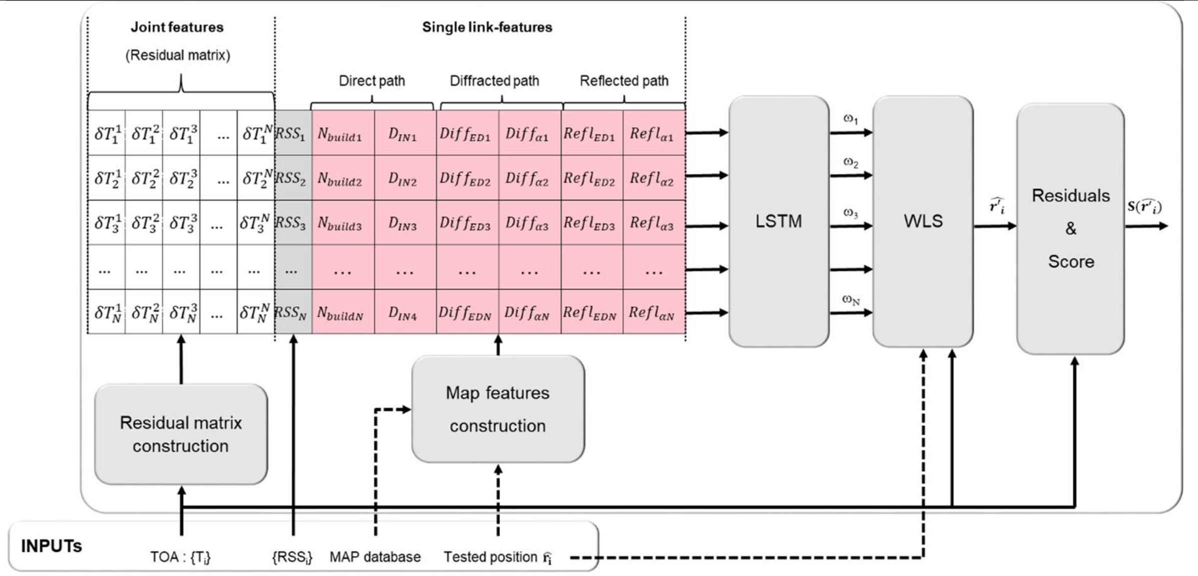

Figure 6 : General architecture for positioning based on map information.

A. Per-link Features

Various per-link measurement features can be enlightening and advantageous as neural network inputs, including gNB height, RSS, and notably, map information.

The gNB height holds significance because signals from lower heights are more susceptible to Non-Line-of-Sight (NLOS) conditions. Low RSS values exacerbate tracking noise, consequently amplifying TOA measurement noise.

Map features introduce complexity due to the extensive spatial area necessitating accurate modeling between the emitter and receiver. All potential obstacles along the wave path can influence propagation, including more distant surfaces via signal reflection. Moreover, any object of comparable length to the wavelength (e.g., 10cm) can potentially interfere with the wave, demanding spatial resolution at commensurate scales in the building model. Balancing the vast areas to model and the minute resolution required results in copious data. For instance, considering a transmission between an emitter and receiver 1km apart, where all buildings within a 500m radius from the midpoint are depicted on an image with a 10 cm resolution (1 pixel corresponding to 10cm), the image size would be approximately 7.8Mpx, necessitating a large neural network for processing.

A preliminary strategy to curtail the volume of input information from the map entails modeling only the surrounding environments of the User Equipment (UE) and the gNB. The underlying assumption posits that signal blockage primarily occurs proximate to the antennas, with obstacles distant from both the emitter and receiver playing a minimal role in propagation. Using the prior example, a 30m-long building situated at the transmission midpoint (i.e., 500m) can be readily bypassed by the wave due to its negligible angular deviation. Conversely, the same building in close proximity to the antenna will impede signal transmission. Regarding the more complex scenario of urban propagation with high building density, it has been observed experimentally that the measured extra path followed by the wave corresponds to a propagation “above the roofs”. It seems that the less attenuated path between two devices is obtained when the wave reflect on buildings faces surrounding e.g. the transmitter until it reaches the top of the buildings, then propagates without any obstacle (i.e. above the roofs), and reflects down on the walls of buildings surrounding the receiver to reach this latter. In that scenario only the buildings close from the transmitter and receiver are determinant.

In a first version, buildings were represented using small (e.g 250 x 250 pixels) “height images” (each pixel contains the height of the building, 0 if there is no building at the given position), each of them modelling the scene around the emitter and the receiver (see Figure 7). Separate images covering the same areas are used to represent the “direct path” ray linking the emitter and the receiver, which indicates the algorithm the direction of arrival.

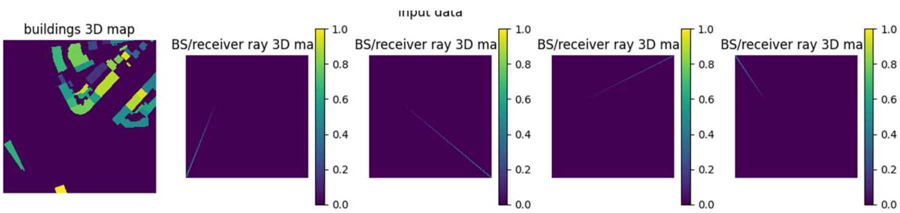

Figure 7: illustration of map representation using height images

However, tests conducted using this map representation were unsuccessful, and this representation has been abandoned.

One possible reason the image-based approach failed is that the input size and complexity were too high relative to the size of the learning dataset, preventing the network from correctly interpreting the information contained in the images. Therefore, we adopted a more compact representation of the map to facilitate the learning of weight predictions.

In this second version, possible interactions of the wave with surrounding buildings are described using ray-tracing methods, but with a limited number of rays used compared to other methods.

Here, the computed rays are :

- The *direct path* (in black in Figure 8)

It is defined as the segment between the gNB and the UE, very straightforward to compute.

- One *diffracted path* (in grey in Figure 8)

In case where there are one or several buildings intercept the direct path, a reflected path is computed. It is defined as the shortest bypass of the blocking buildings between the gNB and the UE, using 2 segments that connect on the edge of one of the blocking buildings, with none of the 2 segments being intercepted by any building from the map. Figure 8 shows the main steps to compute the diffracted path.

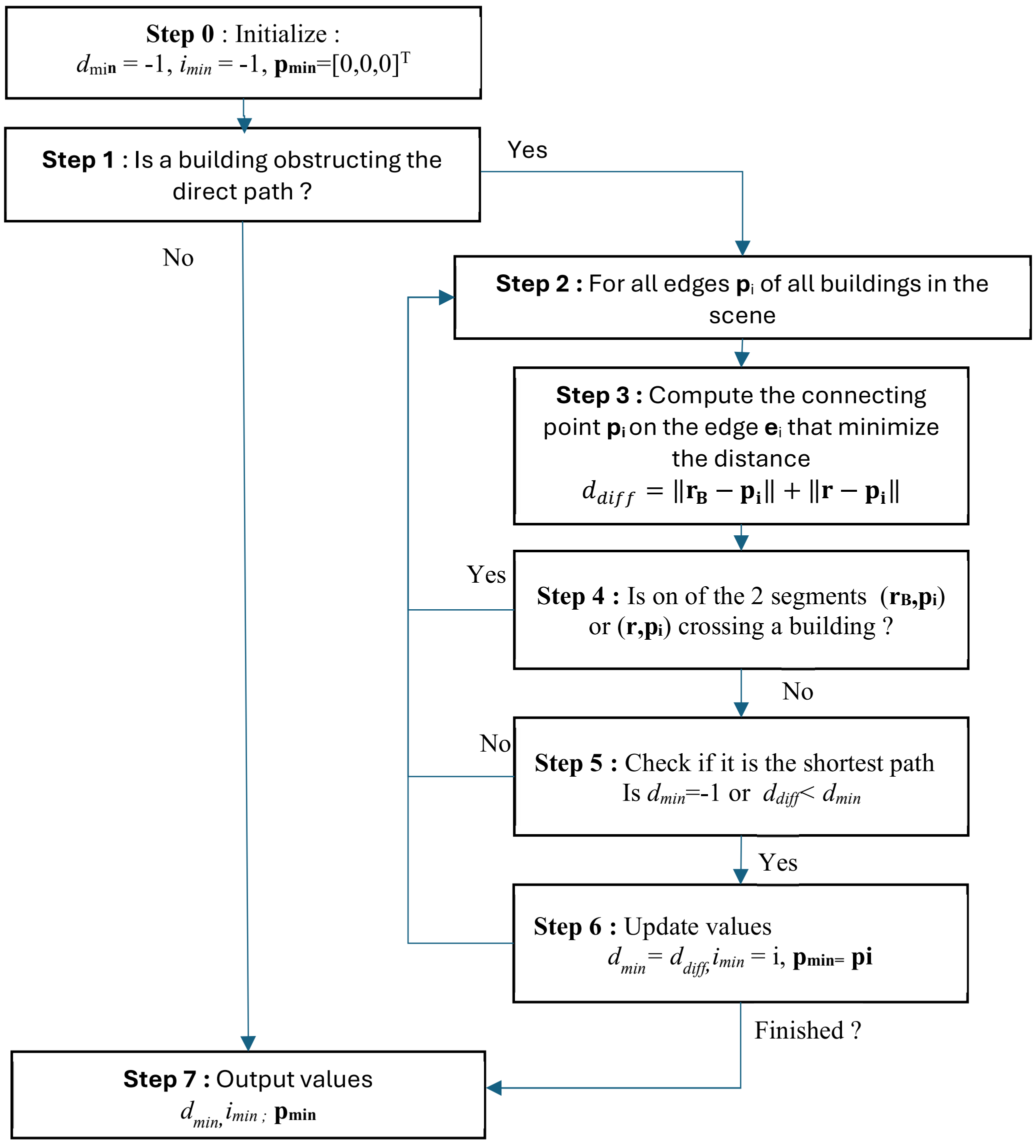

Figure 8 : steps for computing the diffracted path

- One of several reflected paths (in yellow in Figure 10)

Reflected paths correspond to waves that reflect off building faces, often causing significant delays in the TOAs. These paths may be present even when the direct path is detected. Depending on the receiver's ability to discriminate multipath components, they can introduce substantial biases, even under LOS conditions. The number of reflected paths can be unlimited, based on the number of buildings or reflecting surfaces near the receiver. However, we limit the maximum number of reflected paths to a fixed value (e.g., $N_{reflected}$ =2) because we believe the ranging errors are dominated by the "shortest" reflected paths. These are closer to the direct path and harder to discriminate.

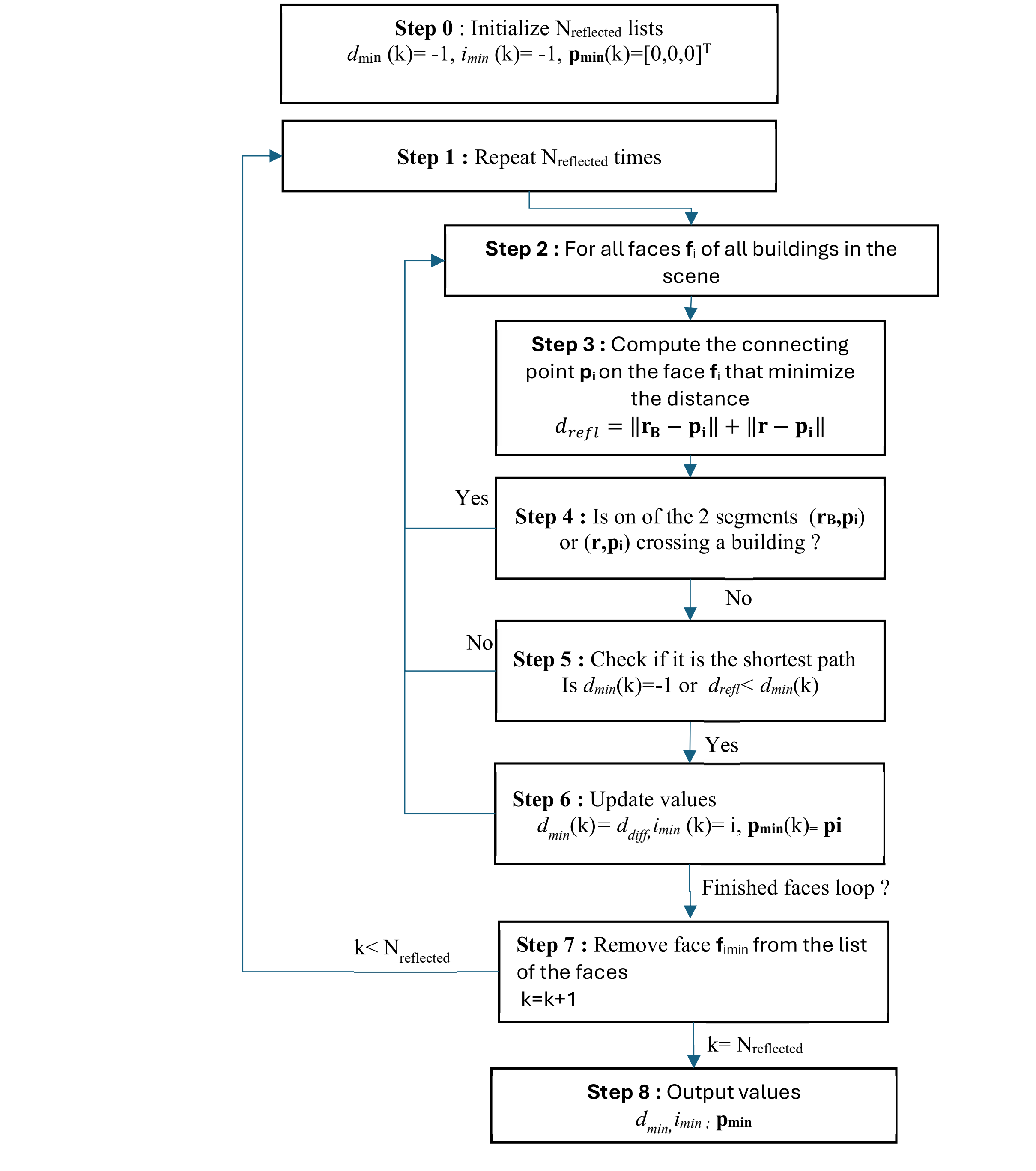

Figure 9 : steps for computing the reflected paths

Reflected paths are defined by two segments between the gNB and the UE, connected on a building face, with neither segment crossing a building. Figure 9 illustrates the steps to compute a reflected path.

Once the direct, diffracted, and reflected paths are determined, the algorithm extracts features that characterize these paths to serve as inputs for the neural network. The idea is that these features capture the main sources of propagation errors, enabling the algorithm to infer the final TOA errors.

Direct Path Features:

- *Direct_Nbuild* ($N_{build,i}$): The number of buildings that intercept the direct path. For example, a value of 3 means there are 3 buildings on the direct path (indicating strong NLOS), whereas 0 indicates LOS propagation.
- *Direct_Din* ($D_{IN,i}$): The distance traveled inside the buildings. When one or more buildings intercept the direct path (*Direct_Nbuild* > 0), this value corresponds to the distance (in meters) of the direct path inside the building. This feature provides information about the "strength" of the NLOS. For instance, a small value (e.g., 50 cm) may indicate that the direct path crosses a building very close to one edge, suggesting the wave is weakly affected by this interaction.

Diffracted Path Features:

- *Diffracted_ExtraDist* ($Diff_{EDi}$): The extra distance traveled by the diffracted path relative to the direct path (i.e., the length of the diffracted path minus the length of the direct path). This indicates the magnitude of the ranging error if the diffracted path is detected instead of the direct path.
- *Diffracted_Angle* ($Diff_{\alpha i}$): The angle between the two rays. This feature indicates the likelihood of the diffracted path being received. For example, an angle close to 180 degrees suggests the two rays almost form a straight line (weak diffraction, with the diffracted path close to the direct path), making it very likely to be received. Conversely, a smaller angle, like 100 degrees, indicates strong diffraction, generally associated with significant signal attenuation, making it less likely to be received.

Reflected Path Features:

- *Reflected_ExtraDist*: The extra distance traveled by the reflected path relative to the direct path (i.e., the length of the reflected path minus the length of the direct path). This indicates the magnitude of the ranging error if the reflected path is detected instead of the direct path.
- *Reflected_Angle*: The angle between the two rays. While this information may be less straightforward to interpret for reflection than for diffraction, it can still be useful.

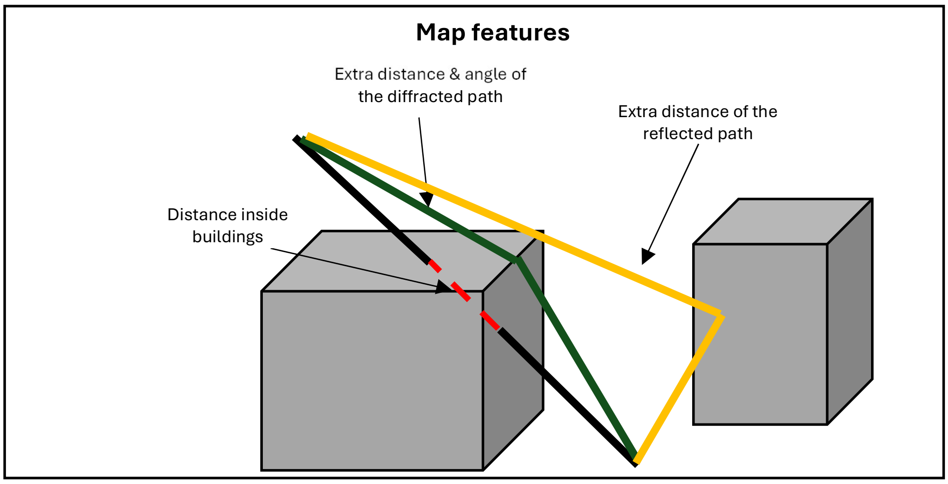

Figure 10 : Illustration of the compact representation of the map.

B. Joint Features

Joint features, which account for the simultaneous impact of multiple measurements over distinct links (as opposed to per-link features), can also be derived from the comparison of positioning solutions from different tested subsets. To address the challenge of testing all possible subset combinations, which is computationally prohibitive, our approach leverages the ability of machine learning to extract hidden interdependencies from only N such subsets. At each navigation epoch, we assume multiple (i.e., N) base station signals are received and a new matrix of positioning residuals M is constructed as follows. We generate N subsets S_n of N−1 TOAs, excluding one distinct TOA measurement (i.e., nth TOA) at a time : $S_n = \{T_i\}_{i=1..N}, i \neq n$. For each subset S_n, we calculate the corresponding solution $\hat{\mathbf{r}}_{\boldsymbol{n}}$ using Eq. 2.4 with equal weights (i.e. $\sigma_{Los/NLOS} = 1$). Then, for each of the N resulting positions $\{\hat{\mathbf{r}}_{\mathbf{1}}, \dots, \hat{\mathbf{r}}_{\boldsymbol{N}}\}$ we calculate the *N* TOA residuals:

$$\delta T_i^n = T_i - h\left(\hat{\mathbf{r}}_{\boldsymbol{n}}, \mathbf{r}_{b_i}\right), i = 1..N \qquad \text{Eq. 2.9}$$

The coefficient $[M]_{n,i}$ (i.e., row n, column i) of the residual matrix *M* is simply given by the corresponding residual δT_i^n.

Each row n of the matrix provides residuals associated with the exclusion of the nth measurement. Although it assumes a single fault per subset (i.e., row), our intuition is that such a matrix can reveal the complex joint contributions of each base station to the positioning solution, while being fed as a single input to the neural network.

C. Long-Short Term Memory Neural Network

The overall input matrix of features fed to the neural network (NN) can be seen as a sequence of N pseudo-observations. At each observation, a single TOA measurement is excluded from computing the solution. By analyzing this sequence, the LSTM NN can exploit the correlations between the excluded measurement and the solution, identifying which measurement exclusions have the most significant impact on the positioning solution's quality. As a result, the NN will be capable of predicting weights that exclude multiple biased measurements by analyzing the sequence of pseudo-observations, set as joint features (see Section III-B).

Additionally, the per-link features for the excluded measurements are concatenated for each pseudo-observation to provide more information about the excluded base stations (see Section III-A).

In these types of problems, the LSTM NN architecture, a type of RNN [20], has the advantage of maintaining memory over multiple (possibly distant) pseudo time steps. Therefore, it is well-suited to exploit the correlations across the matrix rows in our case, even though we explicitly deal with a single epoch problem. Similar applications of the LSTM NN to other time-invariant problems have already been considered. For instance, in [21], LSTM NN was used to process data with long-range interdependence (i.e., using geometric properties of the trajectory for unconstrained handwriting recognition). Note that several other (more complex) neural network architectures were evaluated. For example, we considered a more complex architecture composed of two different concatenated neural networks. The first neural network processes only the residual matrix as input. Its output is concatenated with the additional per-link features and fed as inputs to the second fully-connected NN (FCNN). However, such architectures did not provide any significant improvement over the LSTM NN that only processes the residual matrix. For the sake of conciseness, such alternative architectures are not further discussed in this paper.

2.2 Implementation phase

The scope of LPWAN and the two proposed approaches rely on map information, signal redundancy, and large-scale propagation. Additionally, the AI-based approach requires a substantial database to train the neural network (NN).

To evaluate these map-based approaches, CEA-Leti has deployed a city-wide LPWAN network using LoRa technology instead of NB-IoT. LoRa was chosen primarily for practical reasons : deploying 5G NB-IoT requires licensing and is significantly more costly and complex to implement.

Unlike NB-IoT networks, LoRaWAN networks do not require any authorization, use cost-effective hardware, and achieve comparable ranges to NB-IoT (a few kilometers in free space) with similar bandwidth (e.g., 180 kHz). Moreover, since the focus of the two approaches is on predicting signal quality based on map information, the radio waveform is secondary to propagation in our case.

The main differences between the two technologies that should be considered when interpreting the results are:

- **Carrier Frequency**: LoRa operates at 868 MHz, while NB-IoT covers multiple bands at different frequencies (410 MHz to 7125 MHz).
- **MAC Protocol**: LoRa networks use an unscheduled protocol, meaning transmissions from the UE are subject to significant collision risk and non-negligible packet losses.

TOA Characterization

Some first lab tests have been conducted to qualify the intrinsic TOA detection of LoRa waveforms with respect to NB-IoT.

For these measurements, commercial off-the-shelf (COTS) telecom-grade gateways based on LoRaWAN technology were utilized. Specifically, Kerlink iBTS gateways were employed, which offer fine timestamp measurement capability. This capability, combined with a pulse-per-second (PPS) signal generated by an integrated GNSS receiver, enables the generation of the required TOA metric. Unlike NB-IoT, which requires licensing and regulatory approvals, LoRaWAN does not require any authorization for deployment, making it simpler and less costly to implement.

According to the LoRaWAN specifications, the DataRate (DR) parameter can be adjusted to optimize the trade-off between data rate (high data rate, DR=5 / Maximum Coupling Loss (MCL)=144 dB) and coverage (low data rate, DR=0 / MCL=164 dB). This parameter controls the physical radio characteristics of LoRa and must be considered when characterizing the gateway performances.

The laboratory setup for TOA performance characterization of the gateways across different DR values and Received Signal Strength (RSS) is detailed below.

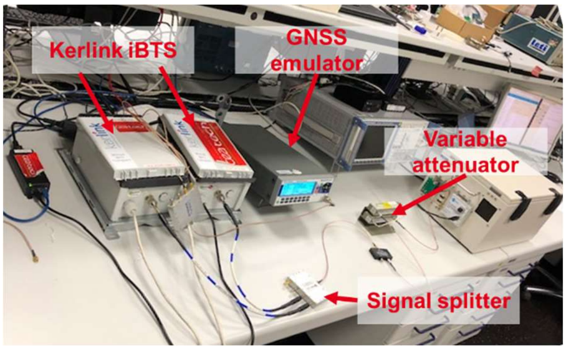

Figure 11 : Setup of laboratory tests for TOA accuracy characterization

A GNSS emulator was configured to send a static GNSS radio signal through a cable plant to two iBTS gateways A and B. The TDOA between the two gateways is defined as:

$$\Delta T_{AB} = T_A - T_B \qquad \textit{Eq. 2.10}$$

Upon packet reception, both gateways should ideally provide the same TOA, resulting in a TDOA of zero. An adjustable RF attenuator was used to control the power received by these gateways. The attenuated signal received by the gateways was generated by a LoRaWAN device configured to continuously send packets, with adjustable DR values.

Dedicated software was used to store the following radio metrics (TOA, Received Signal Strength Indicator (RSSI), and Signal-to-Noise Ratio (SNR)) for each gateway and DR value in a database. Calibration was performed to ensure both gateways provided consistent RSSI and SNR values across all RF attenuator settings.

The TDOA values for DR=5 plotted against RSSI are shown in Figure 12.

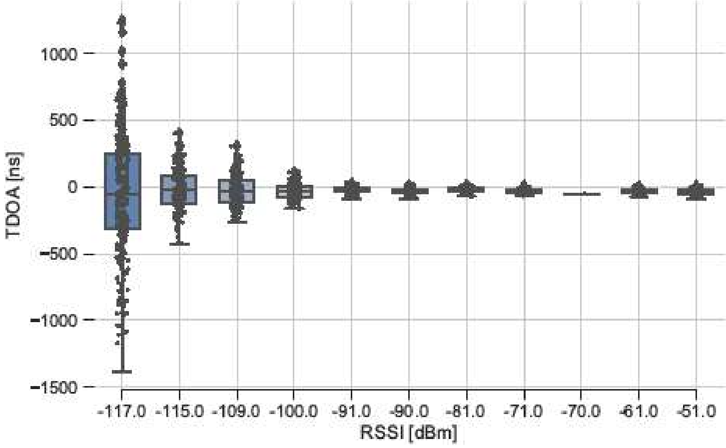

Figure 12 : TDOA values versus RSSI for different DR=5

It can be observed that for high RSS values (>-100 dBm), the standard deviation of TDOA (σ_{TDOA}) is lower than 20 ns, which corresponds to 6m of error, and is to be compared with a typical GNSS PPS jitter value. For lower RSS values (<-115 dBm), σ_{TDOA} increases to more than 300 ns, with some values exceeding 1 µs, representing a maximal error of 300 meters in the worst case. These values are very similar to those reported in (Hu, Berg, Li, & Rusek, 2017), with 68% of errors below 25m and 99% below 300m for NB-IoT.

LPWAN Deployment

The infrastructure comprises six gateways installed around the city of Grenoble through collaboration with several partners. Due to initial site unavailability, some gateways (#4, #5, and #6, see Table 1) were temporarily installed on the roof of a building in the CEA premises named "B2I." This temporary location was very close to gateway #1 (approximately 50 meters away), resulting in poor Geometric Dilution of Precision (GDOP) until they were recently moved to their final locations (#7, #8, and #9).

Taking advantage of Grenoble's mountainous surroundings, some gateways were installed at high altitudes for optimal coverage. Notably, gateways #2 and #3 were installed on the roofs of cable car arrival stations at altitudes of 485 meters and 2259 meters, respectively, providing extensive radio coverage.

#	Name	Alt. (m)	Duration	#packets	Efficency	Coverage
1	BCC @CEA	250	17 months	397 330	61%	58%
2	Bastille	493	17 months	453 448	70%	73%
3	Chamrousse	2259	17 months	323 745	50%	61%
4	B2I-test$_A$ @CEA	236	13 months	188 385	64%	27%
5	B2I-test$_B$ @CEA	236	2 months	26 869	N.A.	N.A.
6	B2I-test$_C$ @CEA	236	2 months	19 610	N.A.	N.A
7	Pont-De-Claix	291	6 months	77 112	21%	22%
8	Vouillants	559	6 months	182 223	51%	51%
9	Alpexpo	232	6 months	141 578	40%	40%
			TOTAL	**1 810 300**		

Table 1 : statisics of deployment

Approximately ten tags were distributed to volunteers for data collection during their daily travels over a period of just over one year. These travels included car, bicycle, and pedestrian movements. The devices embedded GNSS receivers to measure reference positions, which were transmitted along with other data. Each sent packet could be received by one or multiple gateways, which measured various metrics such as tag identifier, Time of Arrival (TOA), Received Signal Strength (RSS), Signal to Noise Ratio (SNR), frequency, etc. These data were recorded in a centralized database for post-processing.
During the ongoing test campaign, a total of 1,810,300 packets have been recorded in the database, nearly three times more than comparable studies (Aernouts, Berkvens, Vlaenderen, & Weyn, 2018).
The data collection zone is confined to an area of 10 km by 15 km, centered on the CEA, which is situated near downtown. Each received packet is assigned to a 10 m by 10 m cell based on its GNSS position. Consequently, the "map" theoretically consists of 1.6 million cells, but only those cells that receive at least one measurement are fully initialized. After 17 months of data collection, this represents a total of approximately 40,000 cells.

Due to GNSS inaccuracies, which can be greater than the cell size, especially in urban environments, a map-matching process is performed before assigning a packet to a cell. This process utilizes the road network from the OpenStreetMap (OSM) database, pre-allocating cells whose locations match specific types of "ways" (as defined by OSM), including streets, highways, hiking trails, etc. When a new packet is received, it is assigned to the closest pre-allocated cell within a 50 m range of its GNSS position. If no such cell is found, the packet is assigned to the nearest cell in the grid.
This approach ensures higher accuracy in mapping and better representation of the actual packet distribution across the area. By leveraging OSM data, the system can account for various types of terrain and pathways, providing a more detailed and realistic depiction of the packet journey. This method is particularly effective in urban areas, where GNSS signals can be obstructed by buildings, resulting in significant positional errors.
Furthermore, the 50 m range for cell assignment is carefully chosen to balance the trade-off between accuracy and computational efficiency. A smaller range could lead to many packets being unassigned due to GNSS errors, while a larger range could increase the likelihood of incorrect cell assignment, thus compromising data integrity. The pre-allocation of cells based on the road network also facilitates better data management and retrieval, as the packets are more likely to be associated with relevant and significant locations.

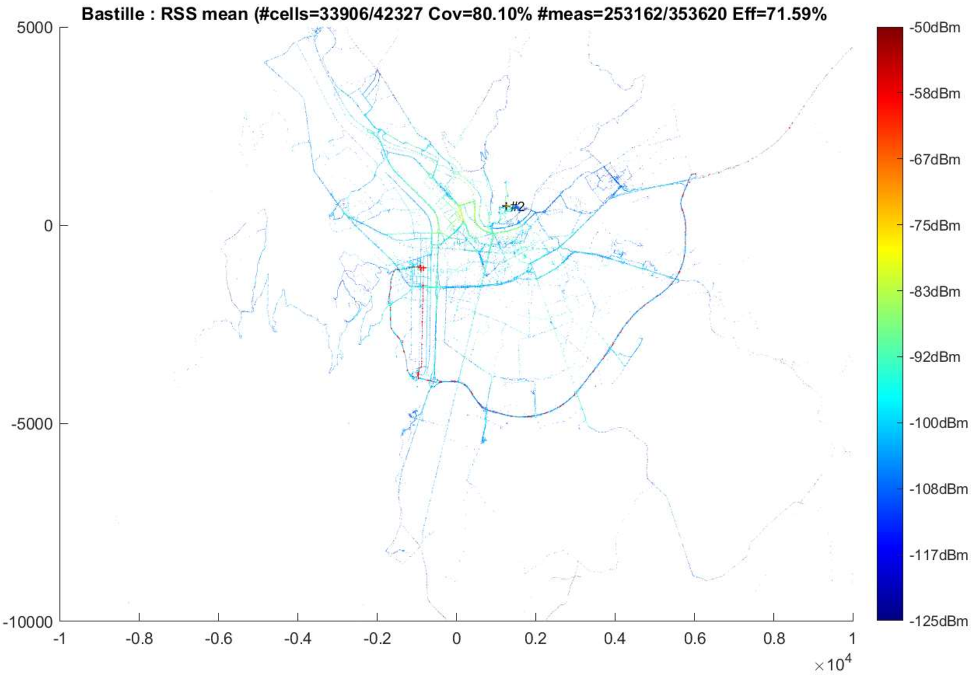

Figure 13: Example of an RSS map for the Bastille gateway. Each dot represents a 10x10m cell where at least one packet has been received. The color indicates the RSS level.

Overall, this meticulous approach to packet assignment enhances the quality of the collected data, making it more reliable for subsequent analysis.

Table 1 shows that the number of packets received varies significantly among gateways, primarily due to their differing activity periods. The coverage corresponds to the ratio between the number of cells for which a given gateway has received at least one packet with respect to the total number of cells for which a packet has been received by any gateway. The efficiency is simply the ratio between the number of packets received with respect to the number of packets transmitted. It is worth noting that the efficiency is relatively low (from 21% to 70%) even for transmissions in the range of a gateway, explained by a significant level of collisions due to the unscheduled nature of LoRaWAN protocol. From the positioning perspective, the main consequence of this issue is that the number of transmissions with at least 3 successful receptions required to compute a position becomes very low. For instance, assuming an average efficiency of 60%, the probability that a packet is successfully received by 3 given beacons is only 21%.

Beyond the laboratory characterization of TOA accuracy, this deployment has allowed us to measure empirical TOA accuracy, marginalized with respect to propagation conditions. In Figure 14, solid lines correspond to LOS and dashed lines to NLOS propagation. These results show two different behaviors depending on whether the gateway is installed at high elevation (e.g., Bastille, Chamrousse) or low elevation (e.g., CEA BCC, CEA B2I). For high elevation gateways, there are no significant differences between LOS and NLOS propagation. As explained in §2.1.2, this can be attributed to the fact that under NLOS conditions, once the signal reaches the "top of the buildings," it can propagate freely to the

high elevation gateway with minimal extra path. Conversely, for low elevation gateways, several obstacles may block signal propagation, causing multiple reflections before reaching the destination, resulting in a significant extra path.
Based on these results, the standard deviation values for the “single-ray approach” (see §2.1.1) have been set to $\sigma_{LOS} = 230m$ and $\sigma_{NLOS} = 1000m$. It is notable that the effective standard deviation values extracted from real-world tests are much higher than those measured during lab tests. This emphasizes the preponderance of propagation conditions over the physical layer in determining localization accuracy.

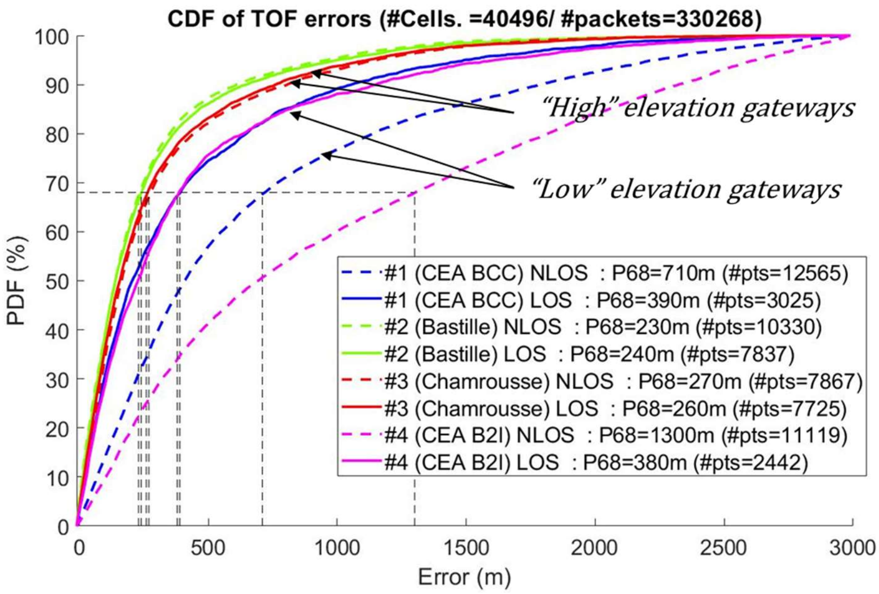

Figure 14: Empirical CDF of TOA errors

2.3 Testing phase

2.3.1 Results for the Single-ray approach

The single-ray approach has been tested under real conditions using the collected measurements from the deployed LPWAN. Due to the technology used for this deployment and data collection, the algorithm was not integrated into the LMF but tested directly using MATLAB post-processing. Out of all the received packets, only a limited number (i.e., 9,925) met the requirements for positioning, which necessitates at least three successful receptions. This limitation is primarily due to the high level of collision inherent to the used protocol.
Figure 15 shows the obtained positioning CDF using this algorithm (in blue) along with the corresponding Cramér-Rao Lower Bound (CRLB), which represents the theoretical performance bound. The positioning accuracy achieved with the algorithm is approximately 2360m, with a theoretical limit of about 510m for 68% of the measurements.

These poor average results are mainly due to the limited robustness of this algorithm. The average errors of NLOS measurements obscure large variations in these errors. When the GDOP is poor, large errors can prevent the algorithm from converging properly, resulting in exaggerated discrepancies from theoretical limits. This highlights the need for more robust algorithms capable of handling the variability and challenges posed by real-world propagation conditions.

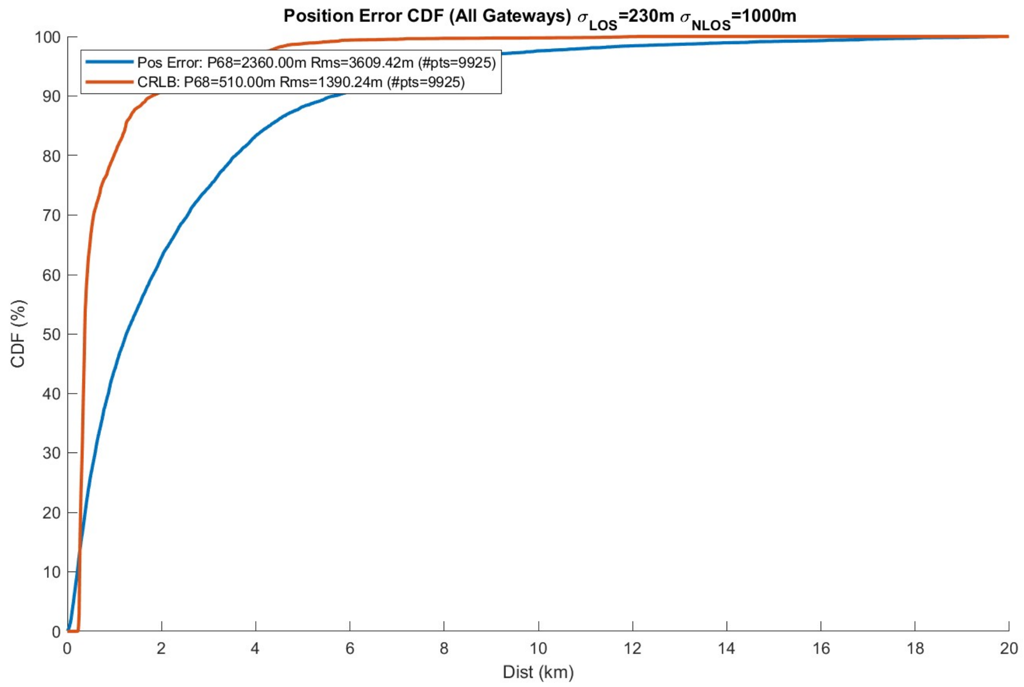

Figure 15 : CDF of the position error using the single-ray approach

2.3.2 Results for the Artificial Intelligence approach

The AI approach requires a significant amount of data for training, validation, and testing. However, the database collected using the LPWAN deployment, despite its large number of measurements, does not meet these requirements. As previously explained, only a limited portion of the collected data is suitable for positioning, restricting the amount of usable data for the AI approach.

To overcome this issue, the algorithm was initially trained on an available GNSS database comprising approximately 12 million measurements. Although GNSS significantly differs from 5G signals (e.g., number of TOA per epoch, TOA accuracy, non-terrestrial propagation), the main concepts of the approach still apply (e.g., unknown user clock but synchronized network, building obstructions). The idea behind this methodology is to perform an initial training based on this GNSS database to develop a preliminary version of the algorithm. In a second step, the neural network is optimized for 5G signals using transfer learning. This two-step approach minimizes the amount of 5G data required for full learning.

The results obtained from the first step are illustrated in Figure 16 which shows the CDF of the errors using the CEA approach (AI-based) compared to a state-of-the-art (SOTA) (Combettes & Villien, 2021) algorithm.

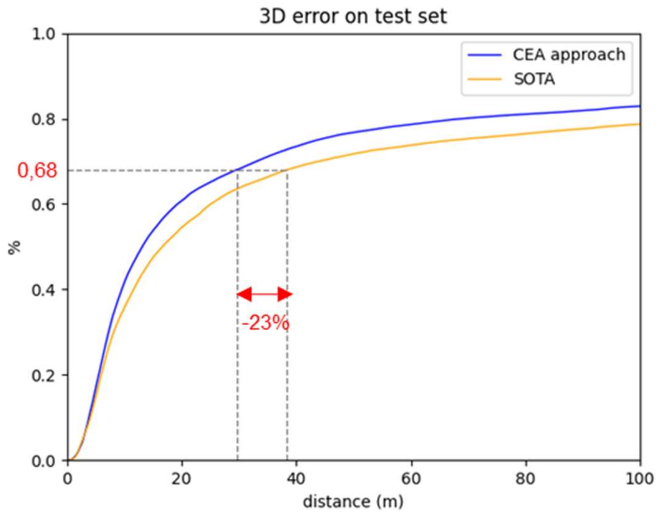

Figure 16 : CDF of errors using AI based approach and the GNSS database

Positioning errors are approximately 30m, a significant improvement compared to those obtained using the LPWA network dataset, primarily due to the inherent accuracy of GNSS measurements. However, when compared to a reference algorithm from the state-of-the-art (SOTA) (Combettes & Villien, 2021), there is a notable 23% improvement attributed to the algorithm itself, particularly in its utilization of map information. This initial finding underscores the promising potential of this approach.

As of the completion of this deliverable, optimization of the algorithm for the LPWAN dataset is ongoing, and specific results are not yet available.

2.4 References

Aernouts, M., Berkvens, R., Vlaenderen, K. V., & Weyn, M. (2018). *Sigfox and LoRaWAN Datasets for Fingerprint Localization in Large Urban and Rural Areas*. Retrieved from https://www.mdpi.com/2306-5729/3/2/13

Combettes, C., & Villien, C. (2021). Ekf based on two fde schemes for gnss vehicle navigation. *IEEE 93rd Vehicular Technology Conference (VTC2021-Spring)*.

Hu, S., Berg, A., Li, X., & Rusek, F. (2017). Improving the performance of OTDOA based positioning in NB-IoT systems. *GLOBECOM 2017-2017 IEEE Global Communications Conference.* Singapore.

3 Positioning in 5G NR using UL-TDoA

The performed work described in this chapter was executed by the Four partners Eurecom, Firecell, TU-Dresden, and Fraunhofer IIS.

3.1 Overview

In this project, we aim to implement 3GPP NR Rel 15 and Rel 16 functionality for positioning/localization in the OpenAirInterface (OAI) radio access network (RAN) as well as the development of advanced positioning algorithms that are especially suited for indoor environments. The main focus of the project is to have an end-to-end uplink time difference of arrival (UL-TDoA) positioning system based on Rel 15 Sounding Reference Signal (SRS) with a localization accuracy of less than 1m in FR1 (sub 6 GHz). The UL-TDoA positioning method [R3.1, Section 8.13] makes use of the Uplink Relative Time of Arrival (UL-RToA) and optionally Uplink SRS Received Power (UL-SRS-RSRP) at multiple reception points (RPs) of uplink signals transmitted from UE. The RPs measure the UL-RToA and optionally UL-SRS-RSRP of the received signals using assistance data received from the positioning server, and the resulting measurements are used along with other configuration information to estimate the location of the UE. The measurements will be provided by the RAN through the NR Positioning Protocol Annex (NRPPa) protocol to the Location Management Function (LMF), which will run the localization algorithms. The simplified network architecture for 5G positioning is depicted in Figure 3.1.

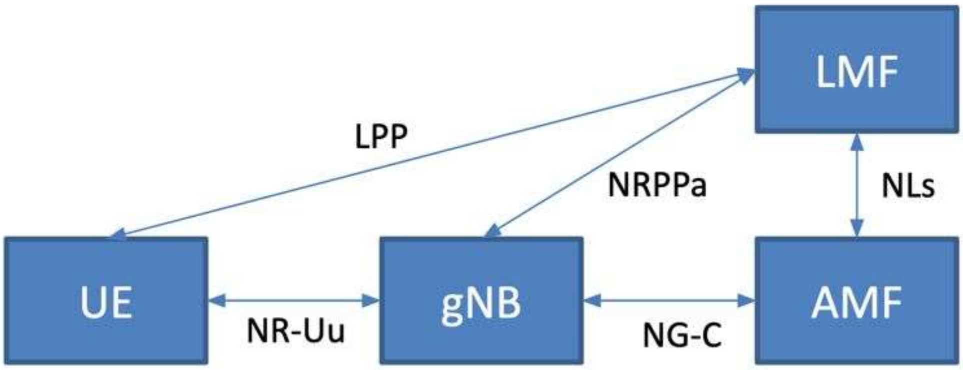

Figure 3.1: Network architecture for 5G positioning

The LTE Positioning Protocol (LPP) covers signaling between UE, the Location Management Function (LMF), and the location server, e.g. Evolved Serving Mobile Location Center (E-SMLC). The Radio Resource Control (RRC) protocol transports the LPP messages over the NR-Uu interface, the NGAP protocol over the NG-C interface, and the HTTP/2 protocol over the NLs interface. The NRPPa defines procedures to transfer positioning-related information between NG-RAN nodes and LMF. It is transported using the NGAP protocol over the NG-C interface and the HTTP/2 protocol over the NLs interface. The detailed operation of the UL-

TDoA positioning method is described in [R3.1, Section 8.13]. A summary of the exchange of messages at each step of the UL-TDoA positioning procedure [R3.1, Section 8.13.3.4] is shown below.

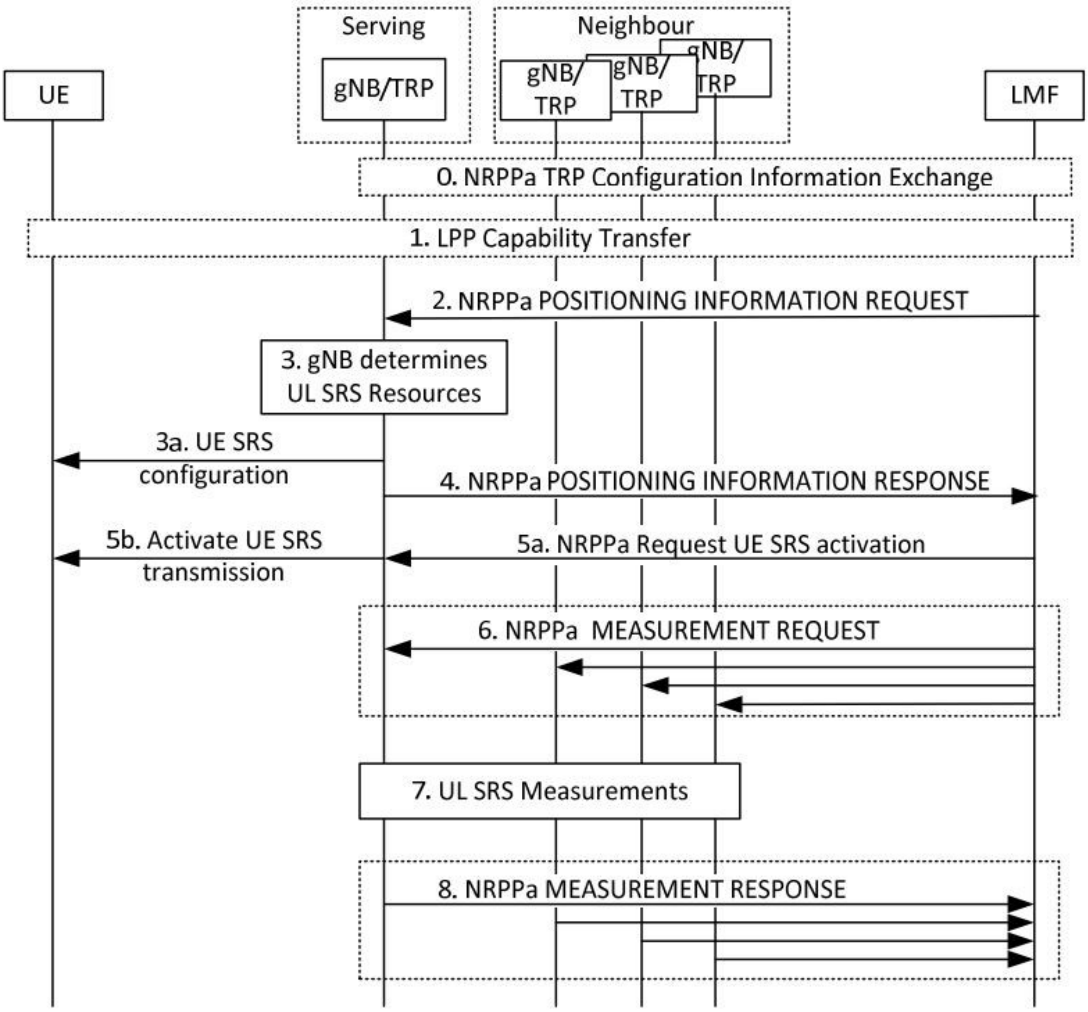

Figure 3.2: UL-TDoA Positioning Procedure (3GPP) [1, 8.13.3.4].

- Step 0: The LMF may use the procedure in [R3.1, Figure 8.13.3.2.1-2] to obtain the TRP information required for UL-TDOA positioning.
- Step 1: The LMF may request the positioning capabilities of the target device using the LPP Capability Transfer procedure as described in [R3.1, clause 8.13.3.1].
- Step 2: The LMF sends an NRPPa POSITIONING INFORMATION REQUEST message to the serving gNB to request UL-SRS configuration information for the target device as described in [R3.1, Figure 8.13.3.2.1-1].

- Step 3: The serving gNB determines the resources available for UL-SRS and configures the target device with the UL SRS resource sets at step 3a.
- Step 4: The serving gNB provides the UL information to the LMF in a NRPPa POSITIONING INFORMATION RESPONSE message.
- Step 5a: The LMF may request activation of UE SRS transmission and sends a NRPPa SRS Activation Request message to the serving gNB of the target device as described in [R3.1, subclause 8.13.3.3a].
- Step 5b: The gNB then activates the UL-SRS transmission. The target device begins the UL-SRS transmission according to the time domain behavior of UL SRS resource configuration.
- Step 6: The LMF provides the UL-SRS configuration to the selected gNBs in a NRPPa MEASUREMENT REQUEST message as described in [R3.1, clause 8.13.3.3]. The message includes all information required to enable the gNBs/TRPs to perform the UL measurements.
- Step 7: Each gNB configured at step 6 measures the UL-SRS transmissions from the target device.
- Step 8: Each gNB reports the UL-SRS measurements to the LMF in a NRPPa Measurement Response message as described in [R3.1, clause 8.13.3.3].

Limitation of OAI source code for 5G RAN and 5G Core (beginning of project)
LMF • LMF Procedures (TS 29.572) • NRPPa Functionalities (TS 38.455) • NRPPa PDU Transfer protocol between AMF/LMF ((TS 29.518) **AMF** • NRPPa PDU Transfer protocol between AMF/LMF (TS 29.518) • NRPPa PDU Transfer protocol between AMF/gNB (TS 38.413) **RAN** • NRPPa Functionalities (TS 38.455) • NRPPa PDU Transfer protocol between AMF/gNB (TS 38.413)

Given the limitation of OAI source code for 5G RAN and 5G Core, the project is divided into the following tasks to achieve its main goals.

3.2 Implementation

In this task, we are extending the current version of OpenAirInterface gNB as well as 5G core with all the necessary functionality so that it can support the NRPPa protocol. Currently, OAI is capable of configuring Rel 15 SRS (UL), channel estimation, and TDoA estimation at multiple gNBs. We are implementing the necessary messages as well as procedures to build the support of 3GPP UL-TDoA positioning [R3.1, 8.13] functionality in OAI.

The partners working in collaboration on the OAI development are Eurecom, Firecell, and TU Dresden.

In this section, we summarize the minimum required functionalities (protocols and algorithms) that are necessary to enable the 3GPP-based UL-TDoA positioning [R3.1, Section 8.13] in OAI and the current status of their development. Figure 3.2 describes the summary of the messages exchanged among several network entities and Figure 3.3 describes the protocol layering for the transfer of NRPPa PDU between gNB and LMF.

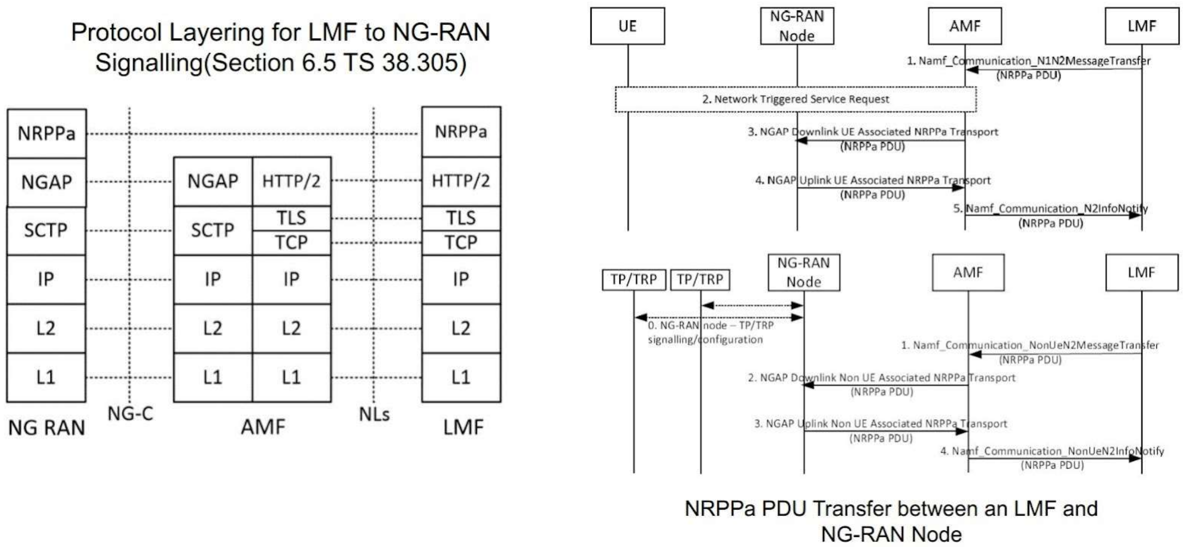

Figure 3.3: Protocol layering for the transfer of NRPPa PDU between gNB and LMF

From Figures 3.2 and 3.3, we can get the following summary of key functionalities that are necessary to enable the 3GPP-based UL-TDoA positioning in OAI.

3.2.1 Required at gNB

At the beginning of the project, OAI gNB does not have any NRPPa functionalities. To enable the 3GPP-based UL-TDoA positioning in OAI gNB, Eurecom and Firecell collaborated and implemented the following functionalities.

3.2.1.1 NRPPa Functionalities (TS 38.455)

List of NRPPa functionalities implemented in OAI gNB	
Function (9.1 of TS 38.455)	Elementary Procedure(s)
Positioning Information Transfer **Status: 1st Version done and Tested**	Positioning Information Exchange Positioning Information Request Positioning Information Response Positioning Information Failure Positioning Information Update Positioning Activation Positioning Activation Request Positioning Activation Response Positioning Activation Failure Positioning Deactivation
TRP Information Transfer **Status: 1st Version done and Tested**	TRP Information Exchange TRP Information Request TRP Information Response TRP Information Failure
Measurement Information Transfer **Status: 1st Version done and Tested**	Measurement Measurement Request Measurement Response Measurement Failure Measurement Update Measurement Report Measurement Abort Measurement Failure Indication

In 1st version, the end-to-end protocol testing with one-gNB and one-UE has been conducted successfully both in simulated setup as well as on Eurecom/Firecell's ORAN Positioning Testbed at Eurecom (refer to [R3.5] for more detail).

3.2.1.2 *NRPPa Transport Procedures 8.10 of TS 38.413*

Status: done and tested

NRPPa PDU Transfer protocol between AMF/gNB (TS 38.413)
• NGAP Uplink UE Associated NRPPa Transport • NGAP Uplink Non-UE Associated NRPPa Transport • NGAP Downlink UE Associated NRPPa Transport • NGAP Downlink Non-UE Associated NRPPa Transport

3.2.2 Required at AMF

Following protocols are required to transport NRPPA PDUs between LMF to gNB through AMF. These protocols have been implemented by the OAI core network team.

3.2.2.1 *NRPPa Transport Procedures 8.10 of TS 38.413*

Status: done and tested

NRPPa PDU Transfer protocol between AMF/gNB (TS 38.413)
• NGAP Uplink UE Associated NRPPa Transport • NGAP Uplink Non-UE Associated NRPPa Transport • NGAP Downlink UE Associated NRPPa Transport • NGAP Downlink Non-UE Associated NRPPa Transport

3.2.2.2 *NRPPa PDU Transfer protocol between AMF/LMF (TS 29.518)*

Status: done and tested

- Development of NRPPa PDU Transfer protocol between AMF and gNB

3.2.3 Required at LMF

At the beginning of the project, the OAI 5G core did not have any LMF. To enable the 3GPP-based UL-TDoA positioning in OAI, TU Dresden has implemented the following functionalities.

3.2.3.1 LMF Procedures (TS 29.572)

- DetermineLocation: Retrieve UE Location (5.2.2.2.2 TS 29.572) (Status: done and tested)
- CancelLocation: Cancel Periodic or Triggered Location (5.2.2.4.2 TS 29.572)

3.2.3.2 NRPPa Functionalities (TS 38.455)

List of NRPPa functionalities implemented in OAI LMF	
Function (9.1 of TS 38.455)	Elementary Procedure(s)
Positioning Information Transfer **Status: 1st Version done and Tested**	Positioning Information Exchange Positioning Information Request Positioning Information Response Positioning Information Failure Positioning Information Update (not done) Positioning Activation Positioning Activation Request Positioning Activation Response Positioning Activation Failure Positioning Deactivation
TRP Information Transfer **Status: 1st Version done and Tested**	TRP Information Exchange TRP Information Request TRP Information Response TRP Information Failure
Measurement Information Transfer **Status: 1st Version done and Tested**	Measurement Measurement Request Measurement Response Measurement Failure Measurement Update (not done) Measurement Report (not done) Measurement Abort (not done) Measurement Failure Indication (not done)

3.2.3.3 NRPPa PDU Transfer protocol between AMF/LMF (TS 29.518)

Status: done and tested

3.2.4 LMF implementation

During the system design phase, Uplink-TDOA (UL-TDOA) was selected as the localization method to be implemented. TU Dresden was responsible to subcontract CampusGenius GmbH with the development of the LMF for the OAI Core. This contract was signed during the year 2022. CampusGenius started the implementation of the LMF for the OAI Core afterwards. CampusGenius is a commercial company developing 5G core technology; therefore, familiar with 5G technology and capable of starting right away.

As the implementation began at the end of the year 2022 in the OAI development branch the University of Hydarabad had provided a LMF branch. During the investigation of this branch, it became apparent that only 1 message had been only rudimentary implemented; thus, the development of the agreed subset of the LMF would be required. This Implementation was done within the project starting December 2022.

NRPPa PDU transfer protocol between AMF/LMF (NAMF) has been implemented from LMF side in cooperation with the AMF team.

Additionally, to the messages and internal logic of the LMF, the interface to an external algorithm for position calculation was developed and implemented. This enables any algorithms to be connected to the LMF and utilize the UL-TDoA information provided by the 5G-System to the LMF. In 5G-Opera this algorithm is provided by the Fraunhofer IIS and has been implemented, verified and tested.

During the development a close cooperation with the AMF and gNB team from Eurecom was established to implement and test the resulting LMF. Those tests have been positive.

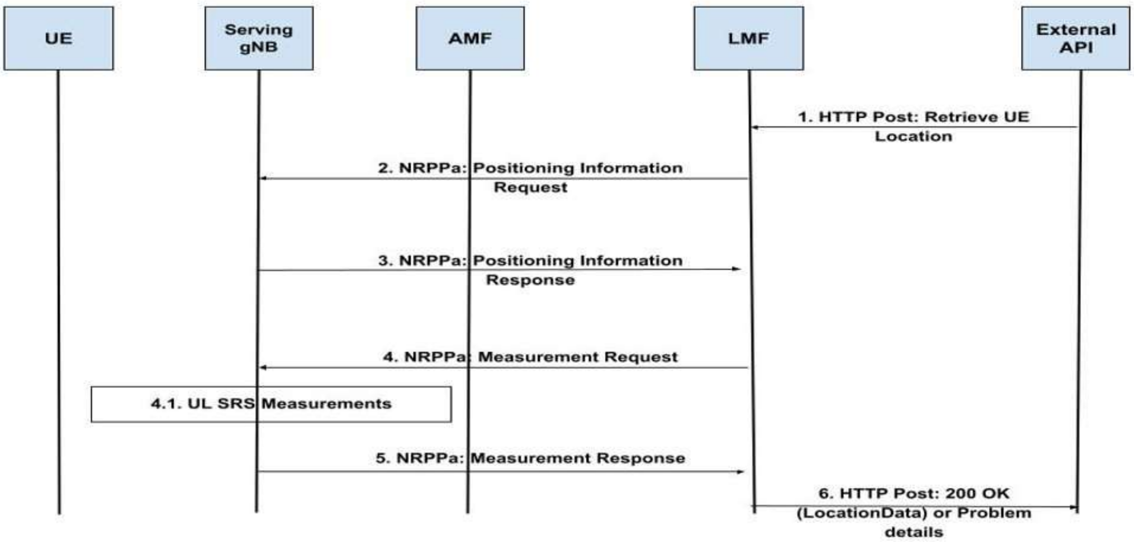

Figure 3.4: Messages Exchange flow between RAN, AMF, LMF and Positioning algorithm.

3.2.5 External API to Initiate Localization

The Determine-Location API in LMF allows a consumer NF (or any External API) to request the location information (geodetic location and, optionally, civic location) for a target UE or to activate periodic or triggered deferred location for a target UE. As shown in Figure 3.5 (Figure 5.2.2.2.2-1 of [R3.2]) to initiate the location procedure, the external API (which can be an advanced API or a simple one-line command) sends the HTTP post request to determine location API, where the request contains a data structure of type InputData (Section 6.1.6.2.2 of [R3.2]).

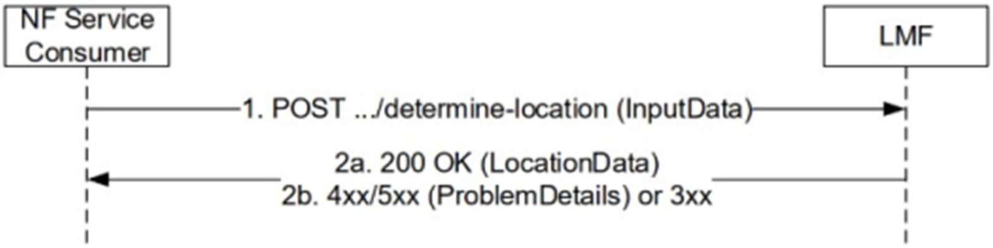

Figure 3.5: Determine Location Request Procedure

We have developed a Python-based external API as well as a simple single command that sends http post request to access the determine-location APIof LMF.

3.3 Positioning Algorithms

3.3.1 Fraunhofer IIS

Fraunhofer IIS, as an experienced specialist in the field of positioning, proposed the localization method “Uplink-TDOA” (UL-TDOA) for implementation. This was because of availability of Reference Signals (namely SRS) already send from commercial 5G NR phones (starting with Release 15). The therefore needed position calculation algorithms for time-of-flight-based positioning to be placed in the LMF of the 5G-Core are implemented by Fraunhofer IIS, too.

The positioning algorithm was created in project year 2023. A so-called "single shot" approach was chosen for this, which can determine a position result based on just one measurement data set with no need for temporal memory or filtering. This makes it easy to integrate into the 5G-Core because it is basically stateless (i.e. has no memory) due to its design as a web service.

Due to legal restrictions, Fraunhofer IIS is currently unable to publish software into Gitlab for the OAI 5G-Core. In order to make the positioning algorithm available to our project partners, provision via Fraunhofer's cloud environment was selected and implemented as a temporal workaround. Figure 3.6 shows the implemented solution.

The partners received the "access client" software, providing access to the cloud service. Partners can use the client to transmit measured time-of-arrival (TOA) values to the server using the "TOA transmitter" module. The position result can then be calculated on the cloud server and is send back to the "positions-receiver" of the "access client".

Furthermore, a "TOA simulator" was developed and added as a module to the "access client". It simulates an infinite circular movement of a UE and determines the theoretically resulting TOA measurement values from the configured "anchor positions" (AP 1 ... AP 4). The 5G radio units will be at those “anchor positions” in a 5G communication system with real hardware.

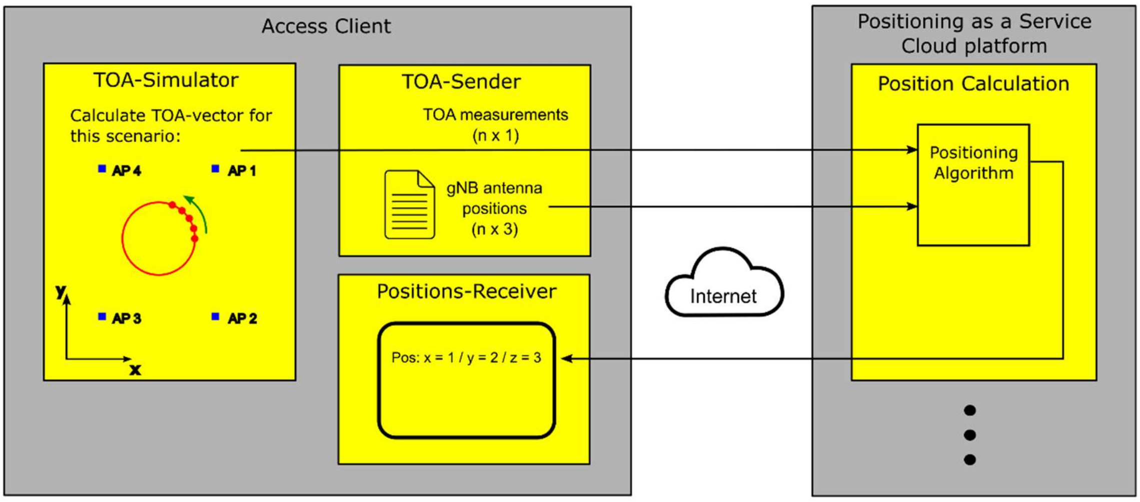

Figure 3.6: Block diagram of the "TDOA positioning" (in the Cloud Platform, on the right) in interaction with the "Access Client" (for communication with the Cloud Server and for generating synthetic measured values, on the left).

3.3.2 Eurecom

- **Currently integrated on LMF:** *pos_est(TDOA,TRP_INFO)*
  - Linear and non-linear methods: LLS, NLS
  - Particle Swarm Optimization: PSO
- **In progress:**
  - Supervised Learning: Fingerprinting
  - Unsupervised Learning: Channel Charting

Position estimation happens on LMF on the OAI 5G Core Network (OAI CN5G). Currently the statistical solutions for position estimation are implemented in C as functions that receive two inputs. First an array of TDoAs and secondly, the relative cartesian coordinates of all TRPs. Following the same format of header file (.h) makes it easy for other partners to contribute to the position estimation.

On the other hand, machine learning methods are dependent on some external libraries such as PyTorch or TensorFlow. Therefore, it is more convenient to use their original implementations in Python on LMF.

3.4 Integration and testing

3.4.1 testing with gNB and rfsimulator

At the beginning of this project, the OAI code does not support the functionalities of LMF and localization-related protocols. Therefore, we adopted several simplifications and developed our first prototype of the system to allow a quick simulation (with rfsimulator) of a simple positioning using UL TDoA based on SRS. The proposed prototype shown in Figure 3.7 aims to replicate as much as possible the actual functionalities with several simplifications, such as a simplified channel model (AWGN), a simplified LMF (Matlab), and an MQTT-based interface (imitating NRPPa) to connect LMF with the gNB directly. The prototype can be used to present the quasi-real-time OAI Rfsimulator-based positioning demo.

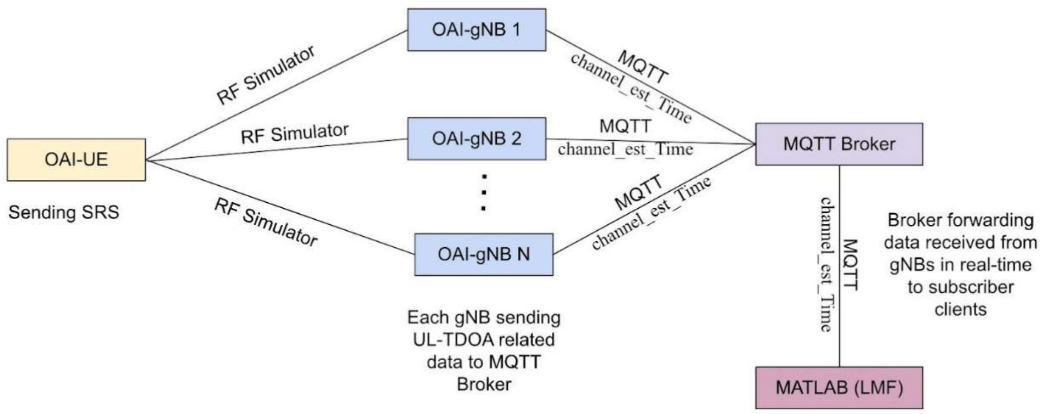

Figure 3.7: Proposed Rfsimulator-Based Simplified Positioning Procedure.

3.4.2 Testing gNB with USRP

In this task, we extend the positioning prototype setting proposed for Task 0 by replacing the Rfsimulator with commercial radios, where we use the Quectel module [R3.3] as UE and USRPs [R3.4] as gNB. Our proposed USRP-based prototype shown in Figure 3.8 allows us to test the UL TDoA-based user positioning without the functionalities of LMF and localization-related protocols (NRPPa/LPP) in OAI.

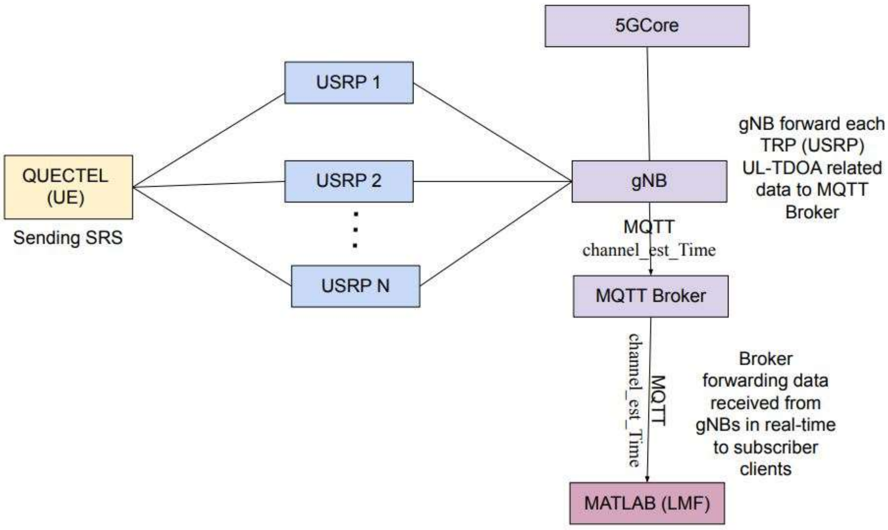

Figure 3.8: Proposed USRP-Based Simplified Positioning Procedure.

3.4.3 testing end-to-end with Firecell RU

The detailed documentation on testing can be found here: https://gitlab.eurecom.fr/geo-5g/docs.git.

3.4.4 Integrating Fraunhofer PaaS to LMF

Adding dependencies and external libraries for AMQP protocol to send TDOAs to Fraunhofer PaaS server and get position estimations in return.
Last commits are pushed to here:

https://gitlab.eurecom.fr/oai/cn5g/oai-cn5g-lmf/-/tree/PaaS?ref_type=heads
https://gitlab.eurecom.fr/oai/cn5g/oai-cn5g-lmf/-/commits/pos_est?ref_type=heads

The performance test with multiple gNBs in rfsim and Firecell RU is in progress.

References:

[R3.1] 3GPP, “Ng radio access network (ng-ran); stage 2 functional specification of user equipment (ue) positioning in ng-ran,” https://www.etsi.org/deliver/etsi_ts/138300_138399/138305/16.01.00_60/ts_138305v160100p.pdf.

[R3.2] 3GPP, "5G System; Location Management Services; Stage 3," 3GPP, Technical Specification 3GPP TS 29.572, 2021.
[R3.3] Quectel, "5g-modules," https://www.quectel.com/product-category/5g-modules.
[R3.4] NI, "Universal software radio peripheral (usrp)," https://www.ettus.com/product-categories/usrp-x-series/.
[R3.5] A. Malik, M. Ahadi, F. Kaltenberger, K. Warnke, N. Thinh, N. Bouknana, C. Thienot, G. Onche, and S. Arora, "From concept to reality: 5g positioning with open-source implementation of ul-tdoa in openairinterface," 2024. [Online]. Available: https://arxiv.org/pdf/2409.05217

4 Novel RTT estimation for 5G NR

This work proposes a Novel RTT estimation method that coherently combines multiple Uplink (UL) Sounding reference signal (SRS) measurements. Compared to the previous works, the inability to exploit multiple UL SRS measurements coherently in the RTT estimation stems from a) inherent timing control loops in 5G NR and b) clock drift. The timing control loops in 5G NR include UL and DL timing control. UL timing control is a continuous process in which gNB sends TA commands to the UE to adjust its UL transmission timing. This procedure is crucial for maintaining UL frame alignment with the gNB. On the other hand, in DL timing control, the UE experiences DL reception timing drift due to clock drift, and it corrects this drift based on DL reference signals and is implementation specific. These timing control loops and the clock drift lead to the variability in delay estimated from SRS measurements obtained in different time slots. Therefore, even in a scenario where the UE is static and the gNB has access to multiple SRS measurements, they cannot be used jointly to estimate the RTT. However, it is well known that multiple measurements improve the estimation performance in low signal-to-noise ratio (SNR) conditions.

In this work, we propose a novel framework to estimate the RTT based on multiple coherent SRS measurements in 5G NR. This approach tremendously improves the accuracy of RTT estimation in low SNR regimes. To the best of our knowledge, accurate RTT estimation without the need for dedicated DL PRS resources is not possible in 5G NR.
Specifically, the contributions of this work are:

- We propose a simple enhancement to the 5G NR signaling scheme that can obtain a sequence of similar UL SRS measurements.
- A matched-filter solution is proposed to estimate the RTT jointly from the collected measurements.
- The proposed method can obtain the RTT even when the 5G UE is in a radio resource control (RRC) inactive state.
- The complete solution is experimentally validated with a real-world 5G testbed based on the OpenAirInterface.

The outcomes of the work are reference in [R 4.1],[R4.2],[R 4.3].

The proposed algorithm in [R 4.1],[R4.2] is validated in real-time using openairinterface in an anechoic chamber as shown in the figure below. The datasets are published in [R 4.3].

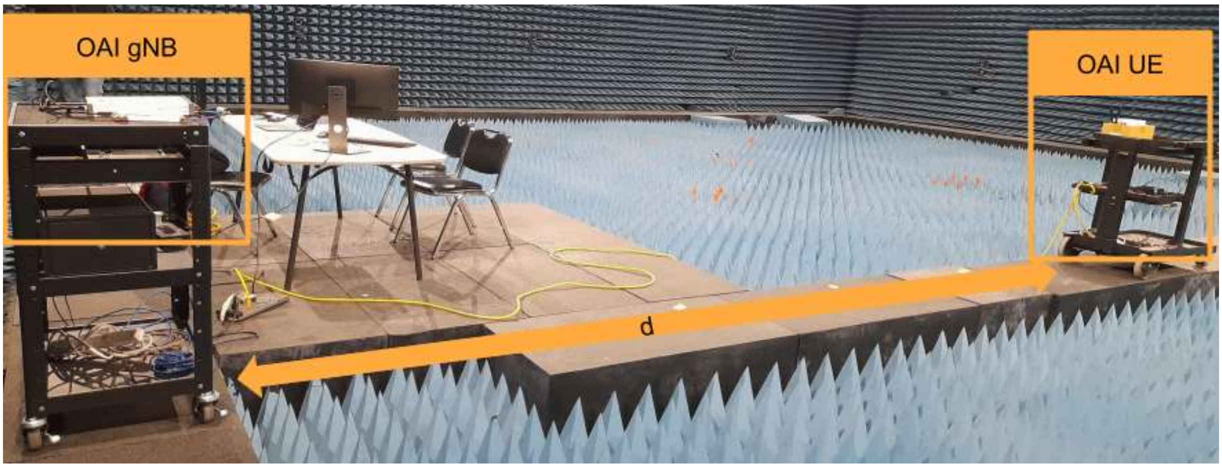

The CDF plots of the accuracy of range estimation at High and Low SNR combining multiple measurements (M) are shown below,

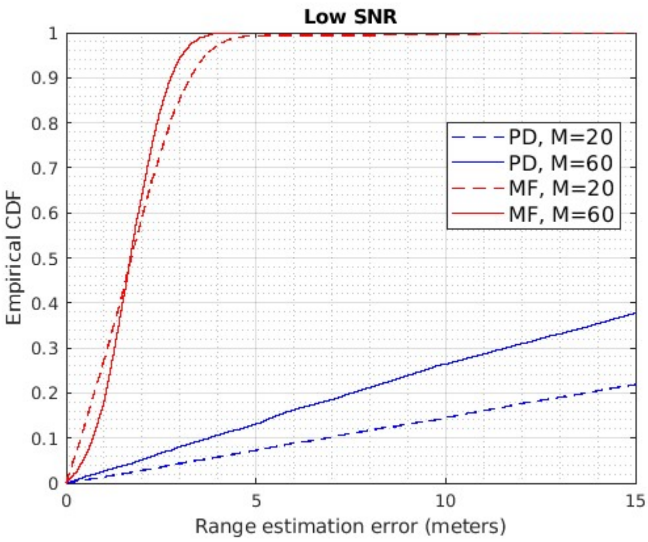

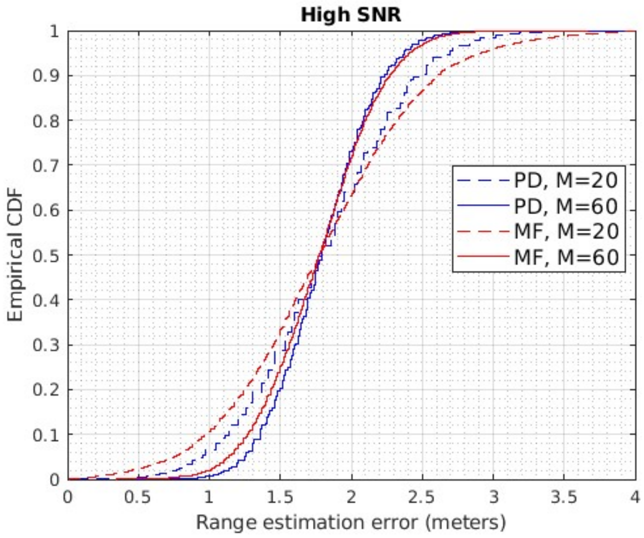

References:
[R4.1] Rakesh Mundlamuri, Rajeev Gangula, Omid Esrafilian, Florian Kaltenberger, Raymond Knopp, David Gesbert, Sebastian Wagner, Trung Kien Le, "System and a Method for Improved Round Trip Time Estimation", EUROPEAN PATENT 23306847.7, October 20, 2023 (accepted)

[R4.2] Rakesh Mundlamuri, Rajeev Gangula, Florian Kaltenberger and Raymond Knopp, "Novel Round Trip Time Estimation in 5G NR", In IEEE GLOBECOM 2024.

[R4.3] Rakesh Mundlamuri, Rajeev Gangula, Florian Kaltenberger and Raymond Knopp, "5G NR Positioning with OpenAirInterface: Tools and Methodologies", accepted in IEEE WONS 2025.

5 Channel Charting for 5G NR

While previously measurements such as ToA and TDoA were used to calculate the position of the UE, Channel State Information (CSI) can offer more detailed channel properties to directly estimate the position from using supervised and unsupervised Machine Learning solutions. Supervised learning, especially fingerprinting (FP) methods, uses a pre-existing database of signal characteristics like CSI or MPC from known locations to train a model for predicting a device's location. This method is effective in stable environments. Unsupervised learning, however, doesn't need a pre-labeled dataset and directly maps data to an objective function, making it suitable for dynamic environments where maintaining a labeled dataset is impractical, allowing it to adapt to changes over time.

Although CSI offers a detailed view of wireless signal propagation, including environmental effects like scattering, fading, and reflection, its high-dimensional data

makes analysis and positioning challenging. Channel Charting (CC) addresses this by creating a map of the wireless medium using CSI, allowing for precise localization and tracking of devices in complex environments.
Channel charting, an application of manifold learning, is crucial for interpreting CSI data. Manifold learning, a non-linear dimensionality reduction technique, uncovers low-dimensional structures within high-dimensional CSI datasets. This enhances the understanding of signal propagation, leading to more precise and efficient perceptions of wireless signal interactions with their environment.
Despite recent advancements in self-supervised CC using deep metric learning, these methods still fall short of the precision achieved by supervised or traditional triangulation methods, even in Line-of-Sight (LoS) conditions. To address this, we developed a novel channel charting algorithm that leverages neural networks and data fusion for accurate user localization. Our specific contributions are as follows:

- We developed a neural network-based channel charting function that accurately localizes users while preserving global geometry.
- We improved localization accuracy by incorporating data fusion with depth data during training.
- Our self-supervised algorithm utilizes nearby Transmission Reception Points (TRPs) and depth data during training without needing labeled data.
- Our method achieves sub-meter localization accuracy with two LoS TRPs 90% of the time, outperforming state-of-the-art and traditional triangulation methods.

Given the CIR dataset, it is possible to find a mapping function that transforms the CIR matrix from multiple antenna measurements to a lower dimension as a proxy for user locations, known as pseudo-positions. Deep neural networks are well-suited for estimating the complex and non-linear mapping function. This way, we build a channel chart algorithm upon a bilateration loss function and by capitalizing on ToA measurements and the location of the TRPs. We extend this method further by incorporating laser scanner data to improve the accuracy of localization. Note that the TRPs locations and laser scanner data are only required during the training phase. Moreover, our approach is self-unsupervised and will provide a global scale representation of the user's location in the global coordinate frame very close to the ground truth as opposed to the pseudo-position of the user.

The table below compares the positioning performance of Classical PSO (min. 3 TRPs) method with different state of the art CC approaches (min. 2 TRPs).

Siamese network uses pairs of CSI measurements and their corresponding Euclidean distance as a dissimilarity metric.

Triplets network encodes triplets of CSI into a 2-D latent space and similar to Siamese, is a semi-supervised and utilizes some labeled data.

Triplets+bilateration Employs a self-supervised approach using known TRPs locations and their received power in a combined triplet and bilateration loss function.

And finally, our approach is a bilateration and laser data fusion shows more accuracy from CSI measurements of only 2 LoS TRPs.

TABLE II: 2 TRPs Comparison of Our Model with State-of-the-Art over Datasets 1 and 2

	CT		TW		CE90 [m]	
Model	1	2	1	2	1	2
Classical PSO	0.987	0.978	0.986	0.984	1.59	1.45
Siamese [12]	0.996	0.994	0.994	0.991	3.08	2.24
Triplets [13]	0.993	0.994	0.992	0.994	2.29	1.35
Triplets+Bilat. [18]	0.991	0.980	0.990	0.964	24.14	22.16
Ours (no Laser)	0.995	0.992	0.995	0.991	3.98	3.81
Ours	0.998	0.996	0.997	0.995	0.94	0.97

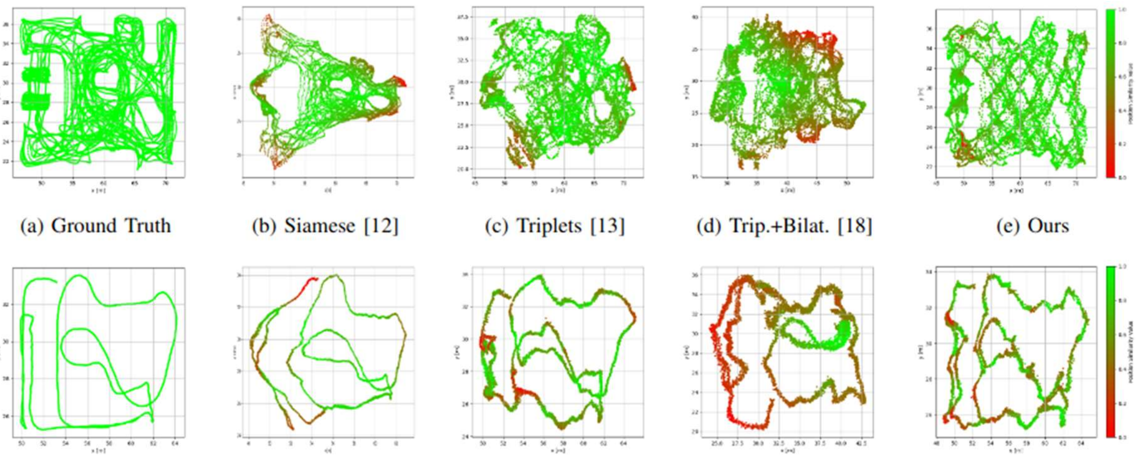

(a) Ground Truth (b) Siamese [12] (c) Triplets [13] (d) Trip.+Bilat. [18] (e) Ours

(f) Ground Truth (g) Siamese [12] (h) Triplets [13] (i) Trip.+Bilat. [18] (j) Ours

Fig. 3: Figures (a) to (e) are the results for test Dataset 1, and figures (f) to (j) are the results for test Dataset 2.

[Global Scale Self-Supervised Channel Charting with Sensor Fusion]

6 Power Delay Profile based Ranging for 5G NR

The orthogonal frequency division multiplexing (OFDM) is widely used in standards such as IEEE 802.11, long-term evolution (LTE), and 5G NR. Consequently, there is increasing interest in leveraging wireless signals for distance estimation and accurate user positioning, especially in environments where GPS signals may be unreliable, such as indoor or complex settings.

We propose a novel Power Delay Profile (PDP)-based ranging method that requires no additional hardware or estimation information. This method exploits the evolution of attenuation over the entire delay spread and captures attenuation at multiple delays (distances), allowing it to account for the curvature of the PDP envelope (the distance-dependent attenuation function). While attenuation is sensitive to calibration errors in synchronization and Tx/Rx gain estimation, the curvature remains insensitive to such offsets. As demonstrated in our previous work [R6.1], PDP-based ranging achieves more precise range estimation compared to RSSI-based methods. However, estimating the PDP envelope from a single channel realization is more challenging than deriving a single RSSI value, as it is sensitive to fast fading, shadowing, scatterer spread, and the fact that the PDP samples its envelope at only a subset of multipath delays. To address this, we exploit the specular part of the channel and focus on the attenuations of the MPC, hence PDP. Another challenge is accurately modeling shadowing in combination with distance-dependent attenuation.

One widely accepted statistical model for indoor multipath propagation is the Saleh-Valenzuela model, which considers reflection, diffraction, and scattering caused by indoor structures. However, this model may not accurately represent channel behavior in outdoor or wide-area environments, as it does not account for wide-area path loss, shadowing, and other outdoor-specific phenomena. For outdoor or wide-area channel behavior, empirical models based on extensive outdoor measurements, such as the Okumura-Hata model or some 3GPP models, are commonly used. Selecting the appropriate statistical model for validation is crucial to ensure its applicability across most cases and confirm that the algorithm used for this model can be extrapolated to others. Compared to alternative models like Rayleigh, Rician, or log-normal distributions, the Nakagami-m distribution demonstrated superior versatility and accuracy in fitting a wide range of experimental data. This is due to its ability to accommodate the superposition of primary and clutter signals resulting from diffuse reflections within a single path, making it more suitable than the Rayleigh distribution. Nakagami-m and Rician distribution models behave similarly near their mean value. However, the Nakagami-m fading model differs from the Rayleigh fading model in that obtaining an analytic form for the likelihood function is impractical due to intractable integrals. Therefore, we concluded that the Nakagami-m decay model is well-suited for validating the feasibility of our PDP-based ranging approach.

Considering the uniform distribution of the phase varying from 0 to 2π for each MPC, we established the relationship between the parameters of the Nakagami-m distribution and the propagation distance to enable distance estimation. The shape parameter m of the Nakagami-m distribution is closely associated with the environment, while the scale parameter represents the average attenuation power intensity, directly linked to the propagation distance. When the received data contains sufficient information about the attenuation of different paths, we can estimate the distance based on these measurements. While many studies have explored the use of MPCs for ranging/localization estimation, to our knowledge, no prior research has focused on directly estimating the propagation distance of the LoS path by assuming that both the LoS and NLoS paths of PDP conform to specific fading distributions.

In formulating the range estimation problem, we found that traditional estimation approaches were inadequate. To overcome this, we proposed the Expectation Maximization (EM) -Revisited Vector Approximate Message Passing (ReVAMP) algorithm. The EM algorithm handles estimation problems with hidden variables. When the analytic formula for the posterior probability density function (pdf) is unavailable within the EM algorithm, we introduce the ReVAMP inference algorithm to approximate the posterior distribution. Compared to the original VAMP, which provides only averaged variances, ReVAMP can yield distinct variances. In ReVAMP, each marginal extrinsic distribution is approximated using a complex Gaussian distribution through approximation belief propagation. Simulations verify the theoretical feasibility of our PDP-based ranging and validate the effectiveness of our EM-ReVAMP algorithm.

However, we must acknowledge that we have not yet collected experimental data to validate the feasibility of our PDP-based ranging, which may lead readers to doubt the generalizability of the Nakagami-m model in other scenarios. Fortunately, the versatility of the EM-ReVAMP algorithm enables our PDP-based ranging to extend to other statistical models besides the Nakagami-m model. Even when transitioning to other fading statistical models, EM-ReVAMP can function with minor adjustments. While we have theoretically validated the superiority of our PDP-based ranging approach over the RSSI approach in our previous work [R6.1], we predict that our approach may not be as precise as state-of-the-art methods requiring additional hardware. The key contributions are following:

- Proposal of a novel PDP-based ranging method requiring no-extra hardware, which focuses on building statistical attenuation models for each MPC in PDP.
- Introduction of the EM-ReVAMP algorithm as a reliable, practical and robust solution for our PDP-based range approach.
- Verification of the superior accuracy and robustness of proposed PDP-based ranging method and EM-reVAMP algorithm with selecting Nakagami-m statistical model through comprehensive simulations.

The outcomes of the work are referenced in [R6.1]. The proposed algorithm in [R6.1] is validated through extensive simulations using Matlab. One simulation result with varying SNR is shown in Figure 6.1.

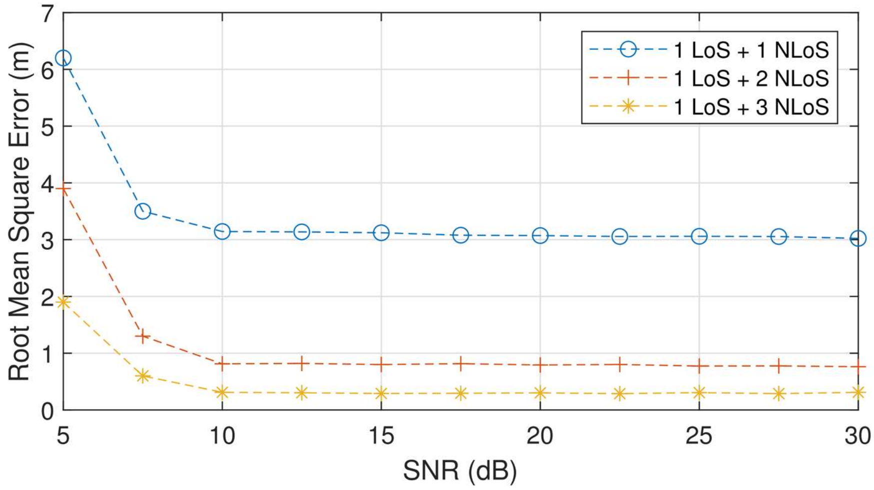

Figure 6.1: The impact of the Nakagami-m distribution's shape parameter m and the number of NLoS paths on range estimation

Based on experimental simulations varying SNR, environmental conditions, and the number of NLoS paths, our method has demonstrated strong performance in diverse and complex environments. The number of NLoS paths has emerged as a crucial parameter significantly influencing estimation accuracy. As this number increases, our algorithm's accuracy improves due to the availability of more eligible samples. Consequently, higher sample counts lead to improved estimation precision. The number of eligible samples used is pivotal in determining the accuracy of our range estimation algorithm, particularly in environments with substantial multipath components where SNR is not particularly low. Thus, in such complex scenarios, the EM-ReVAMP algorithm proves highly effective for estimating LoS distance.

References:
[R6.1] F. Xiao and D. Slock, “A Cramer-Rao Bound for Indoor Power Delay Power based Ranging,” 2023 IPIN-WiP, 25-28 September, Nuremberg, Germany.
[R6.2] F. Xiao, Z. Zhao and D. Slock, "Power Delay Profile Based Ranging via Approximate EM-ReVAMP," 2023 IEEE 28th International Workshop on Computer Aided Modeling and Design of Communication Links and Networks (CAMAD), Edinburgh, United Kingdom, 2023, pp. 31-36, doi: 10.1109/CAMAD59638.2023.10478389.

7 Conclusions

The collaboration between Eurecom, Firecell, TU Dresden, and Fraunhofer IIS in this project has successfully achieved the full implementation of the positioning functionality within the Open Air Interface (OAI) 5G-Software Stack. This collaboration has led to significant advancements of OAI in the following areas:

- **Integration and Testing**: The positioning functionality has been fully integrated and tested within the OAI 5G system, ensuring its operational readiness and reliability.
- **NRPPa Implementation**: The entire NRPPa stack has been implemented within the OAI 5G system, encompassing both the Radio Access Network (RAN) and Core components.
- **LMF Functioning and Testing**: A working Location Management Function (LMF) has been successfully developed, integrated, and tested, confirming its proper operation within the OAI-Core and the 5G-System.
- **Positioning Algorithms:** Basic Positioning algorithms for UL-TDoA have been connected to the 5G-System and can be used within the OAI community.

7.1 Future Work and Expansion

With the foundational work completed, the focus in future projects can shift towards expanding the system in terms of supported messages and algorithms. Future endeavors may include:

- **Enhanced Message Support**: Introducing support for a broader range of localization-related messages to improve system capabilities and interoperability.
- **Algorithm Development**: Developing and integrating more advanced localization algorithms to enhance accuracy, efficiency, and robustness of the system.
- **Performance Optimization**: Continually optimizing the system's performance through iterative testing and refinement.

The successful collaboration has laid a solid groundwork for ongoing and future improvements, setting the stage for further advancements in 5G positioning technologies within the OAI framework.

8 Table of figures